

A comprehensive approach uncovers hidden diversity in freshwater mussels (Bivalvia: Unionidae) with the description of a novel species

Kentaro Inoue^{a,b,*} , John L. Harris^c, Clinton R. Robertson^d, Nathan A. Johnson^e 
and Charles R. Randklev^a 

^aTexas A&M Natural Resources Institute, Texas A&M AgriLife Research Center at Dallas, Dallas, TX, 75252, USA; ^bDaniel P. Haerther Center for Research and Conservation, John G. Shedd Aquarium, 1200 South Lake Shore Drive, Chicago, IL, 60605, USA; ^cDepartment of Biological Sciences, Arkansas State University, Jonesboro, AR, 72467, USA; ^dRiver Studies Program, Texas Parks and Wildlife Department, San Marcos, TX, 78667, USA; ^eWetland and Aquatic Research Center, U.S. Geological Survey, Gainesville, FL, 32653, USA

Accepted 25 April 2019

Abstract

Major geological processes have shaped biogeographical patterns of riverine biota. The Edwards Plateau of central Texas, USA, exhibits unique aquatic communities and endemism, including several species of freshwater mussels. *Lampsilis bracteata* (Gould, 1855) is endemic to the Edwards Plateau region; however, its phylogenetic relationship with other species in the Gulf coastal rivers and Mississippi River basin is unknown. We evaluated phylogenetic relationships, shell morphologies and soft anatomy characters of *L. bracteata* and a closely related congener, *Lampsilis hydiana* (Lea, 1838) throughout their ranges. Our results showed the presence of an undescribed species: *Lampsilis bergmanni* **sp.n.** *Lampsilis bracteata* and *L. bergmanni* **sp.n.** share similar shell morphologies and soft anatomy characters; however, they are genetically distinct. Geological processes, such as faulting and sea-level changes during the Miocene to Pliocene, are likely to have facilitated diversification of *Lampsilis* species, resulting in isolation of *L. bracteata* on the Edwards Plateau and diversification between *L. bergmanni* **sp.n.** and *L. hydiana*. We conclude that *L. bracteata* range is restricted to the Colorado River basin, whereas *L. bergmanni* **sp.n.** occurs only in upstream reaches of the Guadalupe River basin. Conservation actions are warranted for both species due to their restricted distributions and potential anthropogenic threats.

© The Willi Hennig Society 2019.

Introduction

Major geological processes have shaped the current distribution of the world's biota (Avice, 2000; Hewitt, 2000). In riverine systems, isolation by geological vicariance can be profound because stream-dwelling organisms are unable to disperse overland and, therefore, biogeographical patterns of many aquatic species track historical changes in river structure (Hughes et al., 2009). For example, climate-driven sea-level fluctuations can inundate or expose habitat, especially

in the lower reaches of river basins. Likewise, geological events such as faulting or uplift can isolate river segments or bring them together (Woodruff, 1977; Albert et al., 2018). Subsequently, the life history and dispersal ability of species further affect the species distribution. Studies of evolutionary consequences resulting from vicariant events are especially important, given rapid changes in environment due to human-driven climate change and disturbances.

Rivers of the western Gulf of Mexico coastal plain in Mexico and the USA have been shaped by land formation such as uplift of mountain ranges and faulting of rock formations, resulting in a series of isolated river basins that independently drain into the Gulf of

*Corresponding author:

E-mail address: kinoue@sheddaquarium.org

Mexico (Galloway et al., 2011). One area of particular interest for biodiversity research is the Edwards Plateau of central Texas, USA. During the early Miocene (23–16 Ma), land formation along the Balcones Fault and subsidence of the Gulf Coastal Plain resulted in an abrupt topographic change, known as the Balcones Escarpment, creating the Edwards Plateau (Fig. 1; Galloway et al., 2011). Over time, rivers on the Edwards Plateau eroded sediments away to the Gulf of Mexico, exposing rolling hills and creating broad flat valleys. The karst land-structure of the Edwards Plateau contains a number of aquifers and springs creating high gradient streams and providing perennial flows in rivers of the region, including the Colorado, Guadalupe, Nueces and Rio Grande (Woodruff and Abbott, 1979). As a result, rivers on the Edwards Plateau currently harbour unique assemblages of aquatic species, including freshwater mussels, that are distinct from those in downstream portions of Gulf Coastal Plain rivers (Bowles and Arsuuffi, 1993; Randklev et al., 2017).

Freshwater mussels (Bivalvia: Unionidae) reach their greatest species diversity in North America, with about

300 species currently recognized (Graf and Cummings, 2007; Williams et al., 2017). A majority of these species inhabit the Mobile River basin and the Mississippi River basin, which includes major rivers such as the Missouri, Ohio and Tennessee rivers. In contrast, rivers that drain directly into the western Gulf of Mexico tend to be less speciose but often harbour a high number of endemic species (Haag, 2010). The number of Mississippian species begins to decline in central Texas starting in the Brazos River basin and continues to decline through the Rio Grande basin (Neck, 1982). Simultaneously, the mussel fauna increasingly is comprised of endemic species thought to originate from both Mississippian and Mesoamerican affinities (Neck, 1982; Randklev et al., 2017). The large numbers of endemic species and mixture of faunal assemblages in western Gulf coastal rivers represent a transition zone between the mussel faunas of North America and Mesoamerica (Haag, 2010).

Lampsilis Rafinesque, 1820 is the third largest genus in the family Unionidae with 24 species recognized (Williams et al., 2017). Previous molecular phylogenetic analyses revealed that the genus is

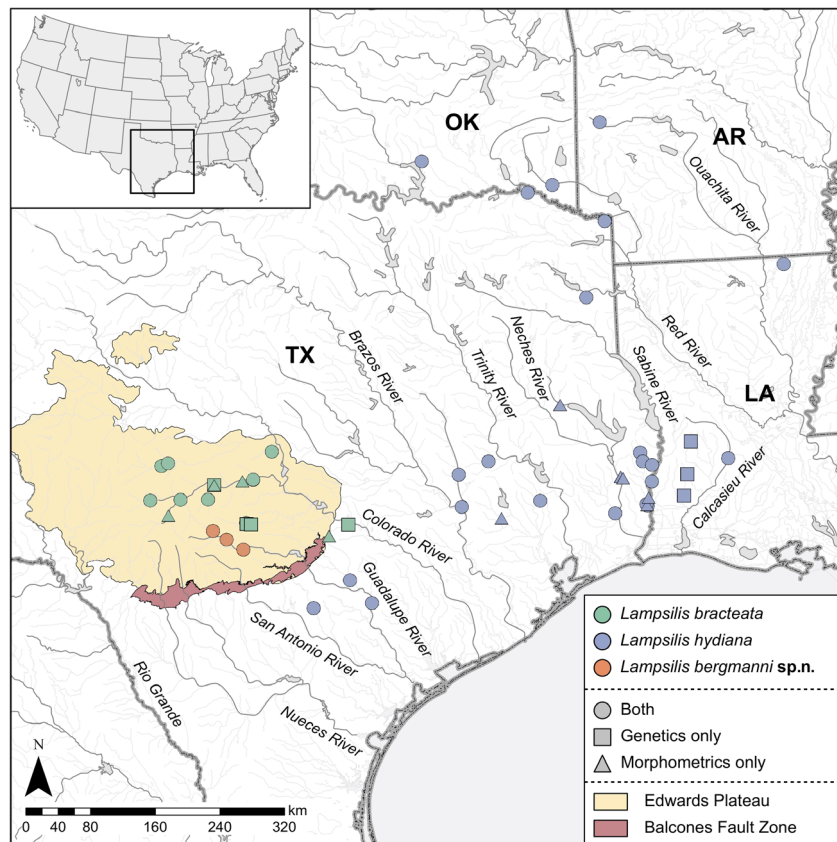


Fig. 1. Collection localities for target taxa specimens used in this study. Colours represent target species (green, *Lampsilis bracteata*; blue, *L. hydiana*; orange, *L. bergmanni* sp.n.). Shapes correspond to specimens used for genetics only (squares), morphometrics only (triangles), or for both genetic and morphometric analyses (circles).

paraphyletic (Campbell et al., 2005; Zanatta and Murphy, 2006); however, many of the species within this group have yet to be validated using modern molecular techniques. The genus is distributed widely throughout North America, including the Hudson Bay, Great Lakes and Mississippi River basins; Atlantic Coastal rivers from Nova Scotia to Georgia; and the Gulf of Mexico coastal rivers from the Florida peninsula to the Rio Grande in Mexico and the USA (Williams et al., 2008). The distributional ranges are varied among species. For example, *Lampsilis streckeri* Frierson, 1927 is restricted to the Little Red River basin in central Arkansas (Harris et al., 2010), whereas *Lampsilis cardium* Rafinesque, 1820 occurs widely in the Red River of the North (Hudson Bay basin), Great Lakes and St Lawrence River basins, and Mississippi River basin ranging from northern Minnesota south to northern Louisiana and from Pennsylvania west to Oklahoma (Vaughn et al., 1996; Watters et al., 2009).

In western Gulf of Mexico coastal rivers, *Lampsilis bracteata* (Gould, 1855) is thought to be endemic to the Colorado and Guadalupe River basins of the Edwards Plateau (Strecker, 1931; Howells et al., 1996). This species was described from the Llano River, a tributary of the Colorado River (Gould, 1855). The disjunct distribution of *L. bracteata* brings into question the taxonomic identity of the Guadalupe River population; however, the phylogenetics and population genetics of the Guadalupe River populations have not been assessed. Therefore, we used *Lampsilis* cf. *bracteata* throughout the study to denote Guadalupe River *L. bracteata*. A second species of interest, *Lampsilis hydiana* (Lea, 1838), thought to be a close congener of *L. bracteata* due to its similar conchological characters and distributional range, occurs in downstream reaches of the Guadalupe River. This species occupies a wide geographical distribution ranging from tributaries of the lower Mississippi River (including the Ouachita and Red rivers in Arkansas, Louisiana, Oklahoma, and Texas) and Gulf of Mexico coastal rivers west of the Mississippi River to the Nueces River, except the Colorado River (Vidrine, 1993; Howells et al., 1996). Although both *L. hydiana* and *L. cf. bracteata* occur in the Guadalupe River basin, *L. hydiana* does not appear to be syntopic with *L. cf. bracteata* and is restricted to lower reaches along the Gulf Coastal Plain downstream of the Edwards Plateau (Howells, 2010). Currently, *L. bracteata* is listed as threatened by the state of Texas (TPWD, 2010) and a candidate for protection under the U.S. Endangered Species Act (USFWS, 2009) due to its low abundance and isolated populations (Randklev et al., 2017). A distribution-wide phylogenetic assessment is necessary to elucidate the taxonomic identity of the putative *Lampsilis* species in western Gulf coastal rivers and to understand

how past geological changes shaped the geographical patterns of the species.

In the present study, we used a holistic approach to evaluate the evolutionary history of the three putative *Lampsilis* species (*L. bracteata*, *L. hydiana* and *L. cf. bracteata*) and make inferences about the role of past geological factors in shaping the current genetic structure and distribution of the species. We included several *Lampsilis* species to assess phylogenetic and phylogeographic relationships of the target species. We first used mitochondrial and nuclear DNA (mtDNA and nDNA, respectively) gene sequences to delineate species boundaries within the three *Lampsilis* species by reconstructing phylogenies and estimating divergence time. Secondly, we used three morphometric methods to examine similarity in shell shapes among the species. Thirdly, we quantified differences in soft tissue anatomical structures among the species. Developing effective conservation strategies and recovery plans requires better understanding of taxonomic status and ecology of target species. Our results clarify *L. bracteata* systematics and taxonomy, which are crucial to state and federal agencies that require defensible taxonomic and biogeographical information to develop conservation strategies for the species.

Methods

Sampling, genetic data collection and estimates of genetic diversity

In this study, we used a total of 54 individuals of *L. bracteata* from five tributaries of the Colorado River, including the type locality in the Llano River; 38 individuals of *L. cf. bracteata* from the Guadalupe River; and 90 individuals of *L. hydiana* from 10 major rivers in Arkansas, Louisiana and Texas for molecular analyses (Fig. 1; Table S1). Samples were collected either as whole specimens or tissue swabs; tissue swabs were collected from foot and mantle tissues by rubbing mucus and epidermal cells using collection swabs (Puritan Diagnostics LLC, Guilford, ME, USA). Live specimens were euthanized with 95% ethanol and then separated into soft tissue and shell. Soft tissues were preserved in 95% ethanol until DNA extraction, and shells were scrubbed inside and out to remove remaining tissue and extraneous material.

We extracted total DNA from mantle tissue clips or tissue swabs using cetyltrimethylammonium bromide (CTAB)/chloroform extraction followed by ethanol precipitation (Saghai-Marooof et al., 1984). Extracted DNA was diluted to 10 ng/ μ L and used as a template in PCRs that amplified the mtDNA cytochrome oxidase I (*cox1*) and NADH dehydrogenase I (*nad1*)

genes and the nDNA internal transcribed spacer 1 (*ITS1*) locus and adenine nucleotide translocase (*ANT*) gene. We used the *cox1* primers described by Folmer et al. (1994), the *nad1* primers described by Campbell et al. (2005), the *ITS1* primers described by King et al. (1999), and the *ANT* primers described by Audzijonyte and Vrijenhoek (2010). We followed the recommended thermal conditions for PCR provided in the original literature. The PCR products were visualized using 1% agarose gel electrophoresis and purified with ExoSAP-IT (Life Technologies Corporation, Carlsbad, CA, USA) or Gen Catch Gel Extraction Kit (Epoch Life Science, Inc., Sugar Land, TX, USA). We employed Eurofins Genomics (Louisville, KY, USA) for DNA sequencing. Sequences were assembled and aligned using SEQMAN PRO v.14.0 (DNASTAR, Madison, WI, USA), and an open-reading frame for the two mtDNA and *ANT* genes was verified. Ambiguous sequences of both the 3' and the 5' end were trimmed. We used MAFFT v.7 (Katoh and Standley, 2013) to perform multiple sequence alignment.

We used DNASP v.5.10 (Librado and Rozas, 2009) to estimate population genetic indices from each locus, including number of haplotypes (*H*), mean number of nucleotide differences (*K*), and mean nucleotide diversity (π) for each putative species and within each major river (Table 1). We used MEGA v.7.0.16 (Kumar et al., 2016) to estimate pairwise genetic divergence (uncorrected p-distance) between pairs of putative species separately for the mtDNA and nDNA datasets.

Phylogenetic analyses

Phylogenetic trees were reconstructed using Bayesian inference (BI), maximum-likelihood (ML), and maximum parsimony (MP) analyses based on a concatenated dataset (*cox1*, *nad1*, *ITS1* and *ANT*). We included 39 species from the tribes Amblemini, Anodontini, Lampsilini, Pleurobemini and Quadrulini to evaluate phylogenetic relationships and used *Arcidens confragosus* (Say, 1829) (Anodontini) to root trees (Table S2). Before the phylogenetic analyses, we used METAPIGA v.3.1 (Helaers and Milinkovitch, 2010) to identify unique haplotypes to save computational time and evaluate substitution saturations for the concatenated dataset. We used only unique haplotypes for the phylogenetic analyses. Phylogenetic analyses were performed with MRBAYES v.3.2.6 (Ronquist et al., 2012), W-IQ-TREE (Trifinopoulos et al., 2016) and MPBOOT (Hoang et al., 2018). Before the BI analysis, we used KAKUSAN4 (Tanabe, 2011) to estimate the best-fit model of nucleotide substitution for *ITS1*, and for each codon partition of *cox1*, *nad1* and *ANT*. Substitution models for each gene partition are described in Table S3. In MRBAYES, two simultaneous Markov Chain Monte Carlo (MCMC) runs (each chain containing three heated and one cold chain) were executed for 5×10^6 generations, with trees sampled every 1000 generations for a total 5001 trees in the initial samples. We used TRACER v.1.7 (Rambaut et al., 2018) to assess the convergence of both MCMC runs by plotting the log-likelihood scores for each sampled point. When

Table 1

Summary statistics for *cox1*, *nad1*, *ITS1*, and *ANT* loci for *Lampsilis bracteata* from five tributaries of the Colorado River, *L. hydiana* from 10 major rivers in Arkansas, Louisiana, Oklahoma and Texas, and *L. bergmanni* sp.n. from the Guadalupe River

Species	Waterbody	<i>cox1</i>			<i>nad1</i>			<i>ITS1</i>			<i>ANT</i>		
		<i>H</i>	<i>K</i>	π	<i>H</i>	<i>K</i>	π	<i>H</i>	<i>K</i>	π	<i>H</i>	<i>K</i>	π
<i>Lampsilis bracteata</i>	San Saba River	1	0.0	0.0000	1	0.0	0.0000	4	0.6	0.0013	2	0.3	0.0007
	Cherokee Creek	1	0.0	0.0000	1	0.0	0.0000	2	2.0	0.0040	2	0.4	0.0007
	Llano River	1	0.0	0.0000	4	0.4	0.0007	4	1.2	0.0026	2	0.1	0.0003
	Pedernales River	2	0.2	0.0002	1	0.0	0.0000	3	1.2	0.0025	2	0.1	0.0003
	Onion Creek	1	0.0	0.0000	1	0.0	0.0000	1	0.0	0.0000	1	0.0	0.0000
	All <i>Lampsilis bracteata</i>	4	0.8	0.0014	4	0.1	0.0002	9	1.3	0.0030	3	0.4	0.0009
<i>Lampsilis hydiana</i>	Ouachita River	4	1.4	0.0022	2	1.3	0.0036	1	0.0	0.0000	2	0.6	0.0012
	Red River	6	2.4	0.0037	5	5.5	0.0092	2	1.3	0.0030	3	0.5	0.0010
	Calcasieu River	2	0.5	0.0008	4	1.3	0.0021	—	—	—	1	0.0	0.0000
	Sabine River	5	1.0	0.0023	4	1.4	0.0024	3	0.7	0.0015	1	0.0	0.0000
	Neches River	8	2.1	0.0034	10	2.8	0.0051	2	0.6	0.0012	1	0.0	0.0000
	Trinity River	2	9.0	0.0139	2	3.0	0.0053	1	0.0	0.0000	1	0.0	0.0000
	San Jacinto River	3	1.2	0.0019	2	1.5	0.0028	3	1.0	0.0025	1	0.0	0.0000
	Brazos River	4	1.0	0.0017	2	0.1	0.0002	1	0.0	0.0000	1	0.0	0.0000
	Guadalupe River	1	0.0	0.0000	1	0.0	0.0000	1	0.0	0.0000	1	0.0	0.0000
	San Antonio River	1	0.0	0.0000	2	0.5	0.0009	1	0.0	0.0000	1	0.0	0.0000
All <i>Lampsilis hydiana</i>	23	1.9	0.0043	22	2.6	0.0053	5	0.7	0.0017	3	0.1	0.0002	
<i>Lampsilis bergmanni</i> sp.n.	Guadalupe River	2	0.5	0.0009	3	1.2	0.0023	1	0.0	0.0000	5	0.6	0.0012
	Overall	27	19.3	0.0460	29	28.9	0.0644	12	3.5	0.0088	8	0.7	0.0016

H, number of haplotypes; *K*, mean number of base pair differences; π , mean nucleotide diversity.

the likelihood values reached a plateau with sufficient effective sample sizes ($ESS > 200$), we considered the Markov chains to be stationary. Accordingly, we discarded the first 25% of trees (1250 trees) as burn-in, and the remaining trees were retained and evaluated using the 50% majority rule for a consensus tree. For the ML analysis, we used auto function in W-IQ-TREE to estimate the best-fit substitution models for each gene and codon partition (Table S3). We used 1000 ultrafast bootstrap replicates to calculate nodal support values (Minh et al., 2013). For the MP analysis, we used default function in MPBOOT to reconstruct the MP cladogram. We used 1000 ultrafast bootstrap replicates to calculate nodal support values.

Divergent time estimates

We used a molecular clock method implemented in BEAST v.2.5.0 (Bouckaert et al., 2014) to estimate divergence time among *Lampsilis* species. We used the concatenated dataset and included 15 putative *Lampsilis* species and *Truncilla macrodon* (Lea, 1859) as the outgroup. A random starting tree was estimated under substitution models estimated by KAKUSAN4 (Table S3). A relaxed lognormal clock model and coalescent-constant-population model were used. We used *cox1* substitution rates available for Unionida (1.68×10^{-9} to 2.86×10^{-9} per substitution site per year; Bolotov et al., 2016). The accuracy of divergent times estimated by molecular clocks has been debated when the divergent times disagree with estimates based on fossil records (Bromham and Penny, 2003). The substitution rates used in this analysis were estimated by a fossil-calibrated phylogeny of *Margaritifera* species and are congruent with rates estimated independently from two *Unio* species currently separated by the Strait of Gibraltar (Froufe et al., 2016). Analysis was run for 5×10^7 generations, with sampling every 1000 generations and a burn-in of 25% of the total saved trees. The remaining trees were retained and evaluated using the maximum clade credibility method for a consensus tree.

Species delimitation analyses

We used a Yule-coalescent method to delimit 15 putative species in the genus *Lampsilis*. We employed two generalized mixed Yule-coalescent (GMYC) models: single-threshold GMYC (ST-GMYC) model (Pons et al., 2006) and Bayesian GMYC (bGMYC) model (Reid and Carstens, 2012). Both GMYC models require ultrametric trees to estimate species boundaries; therefore, we used ultrametric trees generated from BEAST. We used R/SPLITS (Ezard et al., 2013) to conduct ST-GMYC analysis on the consensus tree using the single-threshold method and default intervals. For bGMYC analysis, we randomly selected 100

ultrametric trees from the 37 500 trees after burn-in from BEAST. With R/BGMYC (Reid and Carstens, 2012), we ran 200 000 MCMC generations, sampled the chain every 100 generations and discarded the first 4000 generations as burn-in. We set the threshold parameter priors, t1 and t2, to 2 and 80, respectively, and the starting parameter value at 30. We used a single point estimate approach to delimit species boundaries and set the delimitation threshold relative to the posterior mean of the analysis at 0.5 using the bgmyc.-point function.

Morphometric analyses

We conducted three morphometric analyses—traditional, geometric, and Fourier shape—to compare shell shapes among putative species. We used 79 *L. bracteata* individuals collected from five tributaries of the Colorado River (Cherokee Creek, Llano River, Onion Creek, Pedernales River and San Saba River), 28 *L. cf. bracteata* individuals from the Guadalupe River and 145 *L. hydiana* individuals from 10 major rivers (Table 1 Table S1). For traditional morphometrics, we measured three shell characteristics (maximum length (anterior to posterior), height (dorsal to ventral) and width (right to left valve)) to the nearest 0.1 mm for each individual using digital calipers. To standardize the variables for size, we calculated ratios of the height:length (elongation), width:length (inflation), and width:height (inflation) and normalized using an arc-sine-transformation. For geometric and Fourier morphometrics, we used the right valve of each specimen and took digital photographs with a Canon EOS7D SLR camera (Canon USA, Inc., Melville, NY, USA). We placed each specimen on a log-polar grid with radial lines extending every 5°; the shell was placed such that a horizontal line extended from the anterior of the umbo to the posterior end of the hinge ligament. For geometric morphometrics, we used TPSDig2 (Rohlf, 2018) to place 31 shell landmarks at the intersection of the shell margin and radial lines extending below the horizontal line (Fig. 2a). We used Procrustes transformation to remove size variables from landmark coordinates and set the first two landmarks as homologous landmarks (i.e. landmarks located at the same point on each specimen) and the rest as semi-landmarks (i.e. landmarks located along the margin that slide across specimens) (Zelditch et al., 2004). Using the same digital photographs, we extracted the outline of the shell by cropping the image using PHOTOSHOP CC v.2015.0.0 (Adobe, Inc., San Jose, CA, USA) for Fourier morphometrics (Fig. 2b). Using cropped shell images, the shell outline was described by 20 Fourier coefficients using SHAPE v.1.3 (Iwata and Ukai, 2002).

For all morphometric analyses, we examined morphological variation within and among putative species

through principal component analysis (PCA) and canonical variate analysis (CVA). Although both analyses simplified descriptions of variation among individuals, CVA requires *a priori* assignments to group individuals. Additionally, MANOVA and discriminant function analysis (DFA) were used to determine how frequently principal component (PC) scores correctly distinguished between groups. We created confusion matrices based on the DFA for each morphometric analysis by calculating proportions of correct group assignments. All statistical analyses were performed using the software PAST (Hammer et al., 2001), except that PCA for Fourier analysis was done in SHAPE.

Examination of soft anatomy characters

We used 44 live individuals from the three putative species (13 *L. bracteata* individuals from Cherokee Creek and the San Saba River, 19 *L. hydiana* individuals from Cibolo Creek and the Neches River and 12 *L. cf. bracteata* individuals from the Guadalupe River) to compare soft anatomy structure among species. All individuals were adults and shell lengths range from 48.7 to 76.2 mm (mean = 60.9 mm). For each individual, we removed the right valve with a scalpel and recorded differences in general soft anatomy characters (i.e. soft anatomy overall coloration, labial palp shape and incurrent aperture papillae shape; Fig. 2c).

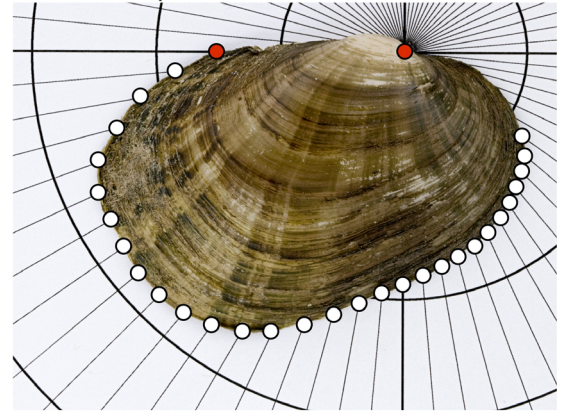
Additionally, we measured 11 anatomical structures (length and height of the right outer gill, right inner gill, right labial palp, and foot; and incurrent, excurrent and supra-anal aperture lengths; Fig. 2c) for each individual to the nearest 0.1 mm using digital calipers. We calculated the proportion of each measurement to shell lengths to standardize for size and normalized using an arcsine-transformation. We examined differences in the anatomical structures among the putative species through PCA and MANOVA. Using biplots of the PCA, we determined anatomical structures providing discrimination among the species. All statistical analyses were performed using PAST.

Results

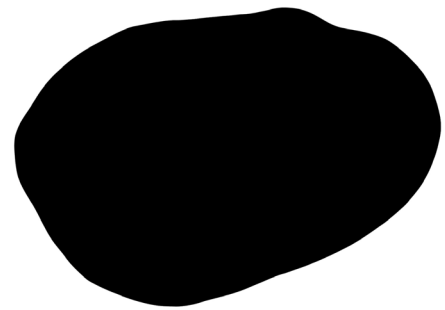
Genetic diversity

We sequenced ~653 bp of the *cox1* gene from 182 individuals, ~599 bp of the *nad1* gene from 175 individuals, ~544 bp of the *ITS1* region from 118 individuals and ~496 bp of the *ANT* gene from 132 individuals. Sequences obtained for this study were submitted to GenBank (accession numbers: MK672001–MK672797; Table S1). *Lampsilis hydiana* had high genetic diversity in mtDNA genes relative to the other species; however, nDNA genetic diversity

(a) Geometric morphometrics



(b) Fourier morphometrics



(c) Soft anatomical characters

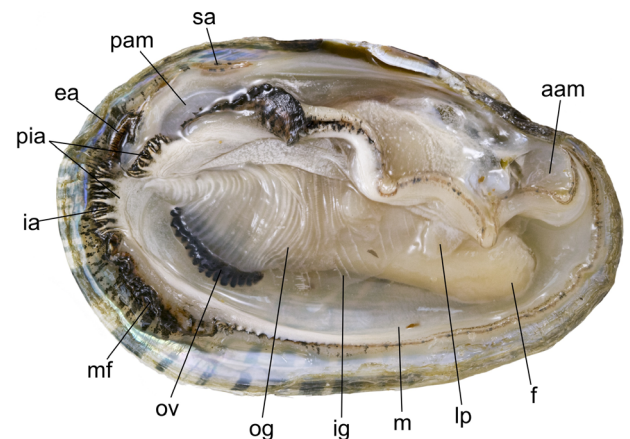


Fig. 2. Right valve with 31 landmarks used for geometric morphometric analysis (a), example of shell outline used for Fourier morphometric analysis (b) and soft anatomical characters (c). Homologous landmarks are indicated by red circles and semi-landmarks are indicated by white circles (a). Codes for anatomical characters are: aam, anterior adductor muscle; ea, excurrent aperture; f, foot; ia, incurrent aperture; ig, inner gills; lp, labial palps; m, mantle; mf, mantle flap; og, outer gills; ov, ovisac; pam, posterior adductor muscle; pia, papillae of the incurrent aperture; sa, supra-anal aperture.

was relatively similar among putative species (Table 1). Pairwise genetic divergence among putative species ranged from 0.0170 (*L. cf. bracteata* vs. *L. hydiana*) to

0.1135 (*L. bracteata* vs. *L. hydiana*; Table 2) for the mtDNA dataset. However, for the nDNA dataset, genetic divergence among putative species was relatively low (range 0.0037–0.0089; Table 2).

Phylogeny

The BI, ML and MP phylogenies based on the concatenated dataset showed similar tree topologies and nodal supports (Figs 3, 4, S1). We did not recover a monophyletic clade of *Lampsilis* species. *Lampsilis* lineages formed two main clades: one with *L. bracteata*, *L. cardium*, *L. cariosa* (Say, 1817), *L. fasciola* Rafinesque, 1820, *L. ornata* (Conrad, 1835), *L. ovata* (Say, 1817) and *L. satura* (Lea, 1852) (hereafter, *Bracteata* Lineage), and the other with *Actinonaias ligamentina* (Lamarck, 1819), *L. higginsii* (Lea, 1857), *L. hydiana*, *L. radiata* (Gmelin, 1791), *L. siliquoidea* (Barnes, 1823), *L. straminea* (Conrad, 1834), *L. teres* (Rafinesque, 1820), *L. virescens* (Lea, 1858) and *L. cf. bracteata* (hereafter, *Hydiana* Lineage). Nominal species generally formed monophyletic clades with strong nodal supports (posterior probability (PP) > 0.99, ML bootstrap support (MLBS) > 95%, MP bootstrap support (MPBS) > 95%); however, *L. cardium* and *L. satura* did not show reciprocal monophyly. In the *Bracteata* Lineage, all trees showed monophyly of *L. bracteata* with strong nodal supports (PP = 1, MLBS = 100%, MPBS = 100%) (Figs 3 4, S1); however, *L. bracteata* formed a basal clade of the *Bracteata* Lineage in the ML and MP trees (Figs 3 4), whereas the BI tree showed a polytomic relationship among species within the *Bracteata* Lineage (Fig. S1). In the *Hydiana* Lineage, *A. ligamentina* was nested within the lineage and sister to *L. higginsii* (Figs 3 4, S1). *Lampsilis hydiana* formed a monophyletic clade, which is sister to a clade of *L. straminea* and *L. virescens* in the BI and ML trees (Figs 3 S1), whereas the MP tree showed *L. hydiana* sister to *L. cf. bracteata* (Fig. 4); however, nodal supports were relatively weak (PP = 0.79, MLBS = 92%, MPBS = 88%) (Figs 3 4, S1). *Lampsilis cf. bracteata* formed a monophyletic clade with strong nodal supports (PP = 1, MLBS = 100%, MPBS = 100%). Neither *L. bracteata* nor *L. hydiana* showed clear geographical structure within species (Figs 3 4, S1).

Divergent time estimates

A time-calibrated phylogeny generated from BEAST was generally congruent with the BL and ML phylogenies (Fig. 5); however, the BEAST tree showed that *L. cf. bracteata* was a sister clade to *L. hydiana*. We did not recover a monophyletic *L. cardium* or *L. satura*; thus, we collapsed the clade comprising *L. cardium* and *L. satura* (collectively hereafter, simply *L. cardium* based on priority; Fig. 5). Major diversification of *Lampsilis* lineages likely occurred during the Oligocene to Pliocene epochs (30–2.58 Ma; Fig. 5). The median estimate of the split between the *Bracteata* and *Hydiana* lineages was 28.2 Ma (95% credible interval: 34.3–22.1 Ma; Fig. 5). *Lampsilis bracteata* diverged from other species within the *Bracteata* Lineage 23.4 Ma (29.7–17.2 Ma) with relatively high nodal support. The *L. fasciola* and *L. ornata* clade diverged from the clade including *L. cardium*, *L. cariosa* and *L. ovata* 19.7 Ma (24.4–14.3 Ma) followed by divergence between *L. fasciola* and *L. ornata* 18.2 Ma (21.1–11.1 Ma); however, nodal supports for these clades were rather weak. Divergence among *L. cardium*, *L. cariosa*, and *L. ovata* occurred more recently, ranging from 7.1 Ma (9.7–4.6 Ma) to 5.7 Ma (7.0–2.8 Ma). In the *Hydiana* Lineage, *L. higginsii* formed a basal clade and diverged from other species 20.9 Ma (26.3–15.6 Ma) followed by the divergence of *L. teres* 20.3 Ma (23.3–13.7 Ma). Diversifications among *L. hydiana*, *L. straminea*, *L. virescens* and *L. cf. bracteata* likely occurred in the late Miocene to Pliocene from 5.5 Ma (7.5–3.6 Ma) to 3.0 Ma (4.3–1.9 Ma).

Species delimitation analyses

Species delimitation analyses based on two Yule-coalescent methods identified 14 putative species within *Lampsilis*. Both methods recognized the undescribed *L. cf. bracteata* as a distinct taxon, and *L. cardium* and *L. satura* to be conspecific.

Morphological variation among putative species

We examined shells from 252 individuals for the morphometric analyses. For traditional morphometrics, the

Table 2

Mean pairwise genetic divergences (uncorrected p-distance) for the concatenated mitochondrial DNA (below diagonal) and the concatenated nuclear DNA (above diagonal) sequences from *Lampsilis bracteata*, *L. hydiana* and *L. bergmanni* sp.n.

	<i>Lampsilis bracteata</i>	<i>Lampsilis hydiana</i>	<i>Lampsilis bergmanni</i> sp.n.
<i>Lampsilis bracteata</i>	—	0.0064 (0.0021)	0.0089 (0.0030)
<i>Lampsilis hydiana</i>	0.1135 (0.0092)	—	0.0037 (0.0016)
<i>Lampsilis bergmanni</i> sp.n.	0.1084 (0.0092)	0.0170 (0.0034)	—

Standard deviations are shown in parentheses.

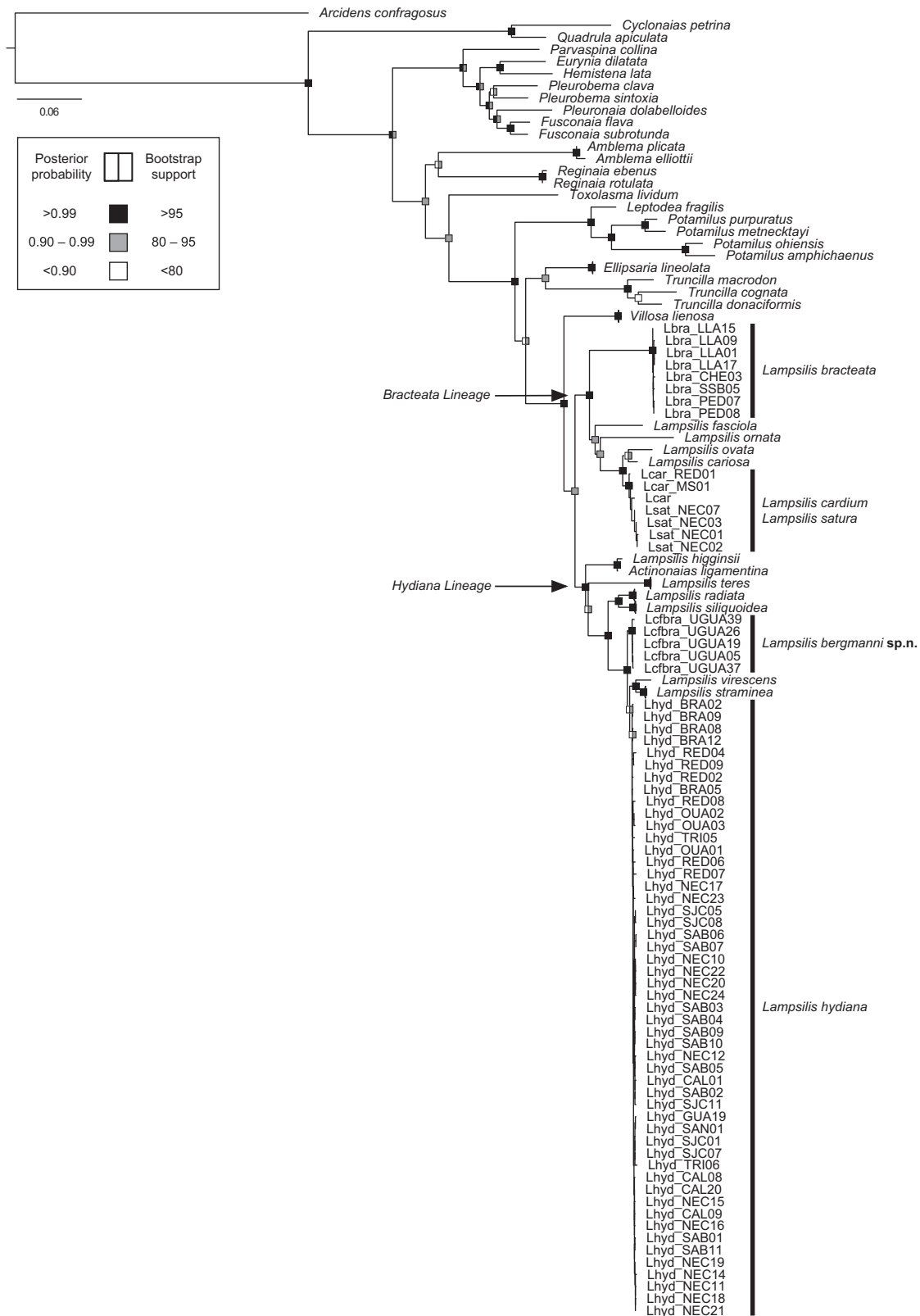


Fig. 3. Phylogenetic tree reconstructed by maximum-likelihood (ML) analysis for the concatenated mitochondrial DNA (*cox1* and *nad1*) and nuclear DNA (*ITS1* and *ANT*) sequence dataset. Nodal supports (i.e. posterior probability values from Bayesian analysis and bootstrap support values from ML analysis) are shown in shaded squares along the nodes. The tree was rooted with *Arcidens confragosus*. Major clades are annotated.

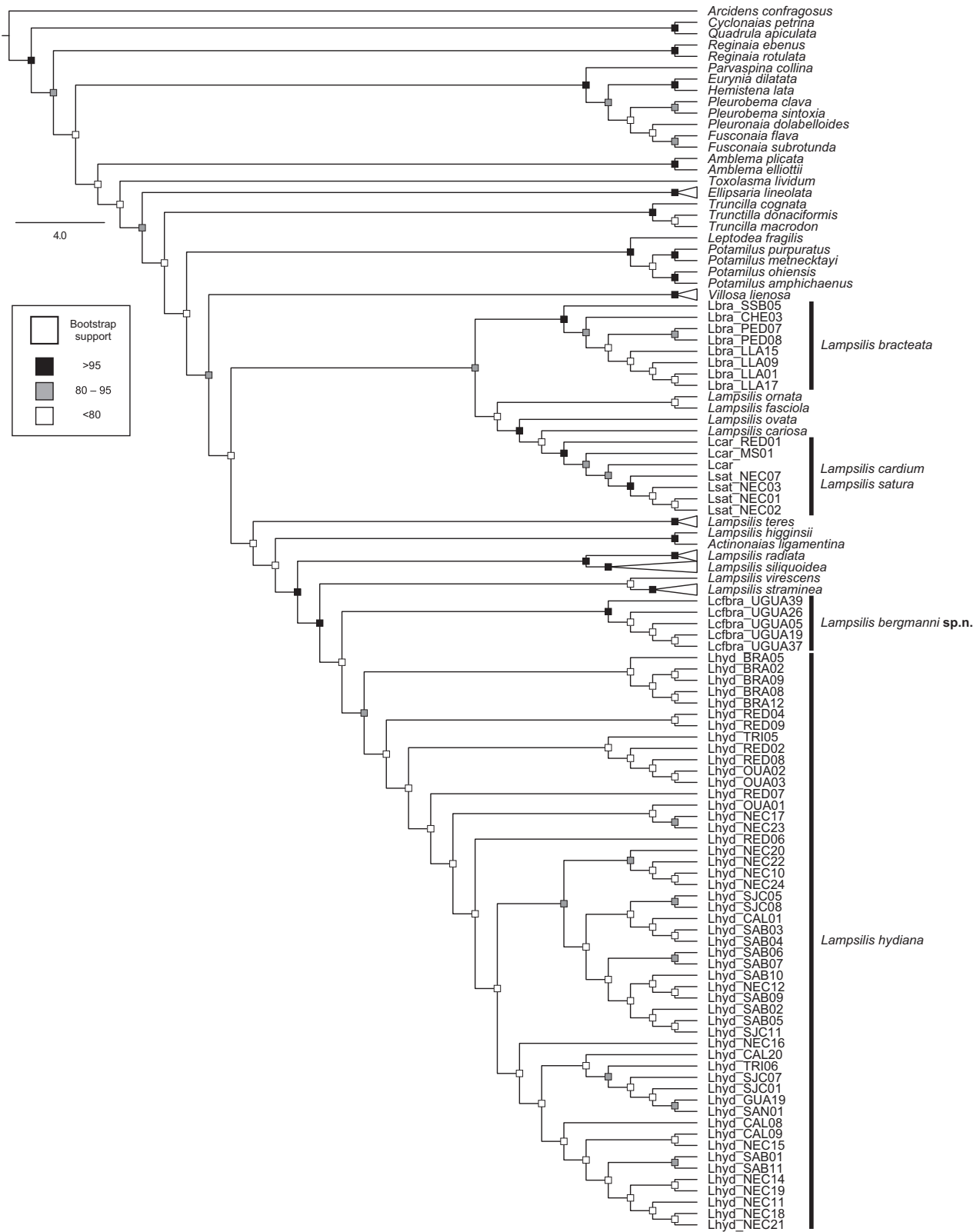


Fig. 4. Maximum parsimony cladogram for the concatenated mitochondrial DNA (*cox1* and *nad1*) and nuclear DNA (*ITS1* and *ANT*) sequence dataset. Bootstrap support values are shown in shaded squares along the nodes. The tree was rooted with *Arcidens confragosus*. Major clades are annotated.

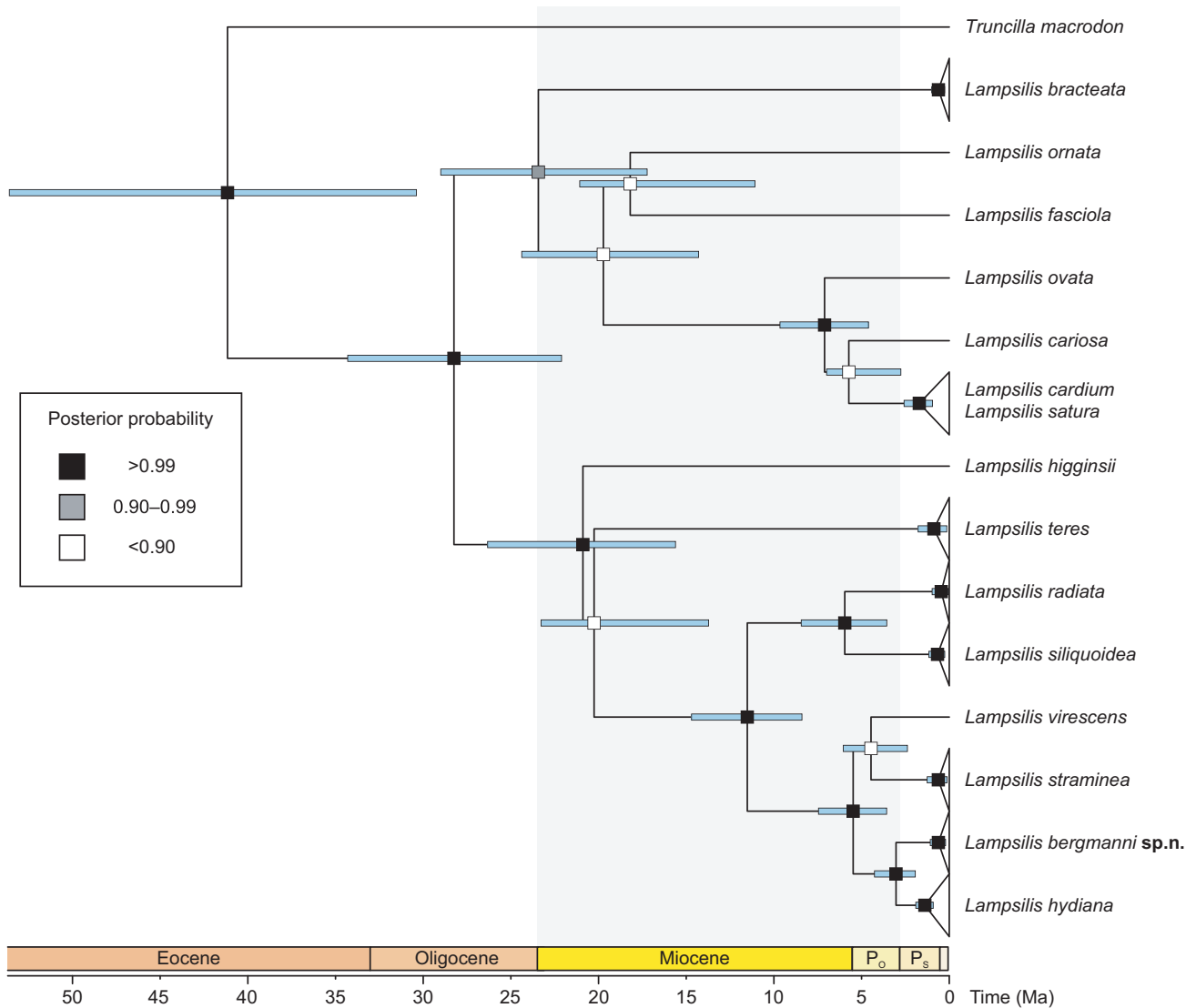


Fig. 5. Maximum clade credibility tree based on the concatenated mitochondrial DNA and nuclear DNA sequence dataset analysed from BEAST. Divergence time is scaled to million years ago (Ma). Bayesian posterior probability values are shown in shaded squares along the nodes (white < 0.90, grey = 0.90–0.99, black > 0.99). Horizontal bars represent 95% credible intervals. Grey shade represents the Neogene subperiod (23.03–2.58 Ma). P_o, Pliocene; P_s, Pleistocene. *Lampsilis cardium* and *L. saturata* were collapsed into a single clade.

PCA yielded two distinct eigenvalues that described > 99% of the total variation among individuals (Fig. 6a). The PC1 axis described 86% and the PC2 axis described 14% of the total variation. The PCA plot with group assigned by species showed that *L. hydiana* had larger morphological variation relative to *L. bracteata* and *L. cf. bracteata*, and the species clusters overlapped

(Fig. 6a). Similar to PCA results, CVA clusters showed wide morphological range of *L. hydiana* and overlap among species clusters (Fig. 6b). The MANOVA showed significant differences between shell morphologies of the mean of each species (Wilk's $\Lambda = 0.766$; $F_{6,496} = 11.9$; $P < 0.001$), except between *L. bracteata* and *L. cf. bracteata* ($P = 0.755$). Mean correct

Fig. 6. Biplots from principal component analysis (PCA) and canonical variate analysis (CVA) of traditional (a, b), geometric (c, d) and Fourier (e, f) morphometrics. Colours and shapes of points correspond to putative species (green circles, *Lampsilis bracteata*; blue squares, *L. hydiana*; orange diamonds, *L. bergmanni sp.n.*). Polygons enclose convex hulls of each species. Biplots of variables from traditional morphometrics (a) are shown in arrows (HL, height:length; WL, width:length; WH, width:height). Deformation grids from geometric morphometrics (c) represent mean shape (top-right) and $\pm 2 \times SD$ on PC1 and PC2 axes. Outlined shell shapes from Fourier morphometrics (e) represent mean shape (top-right) and $\pm 2 \times SD$ on PC1 and PC2 axes.

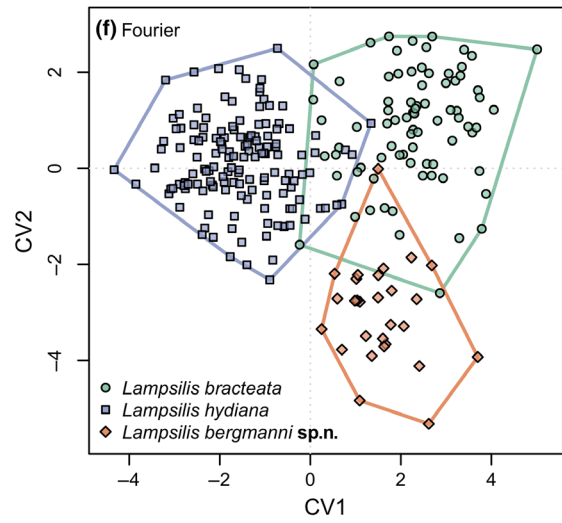
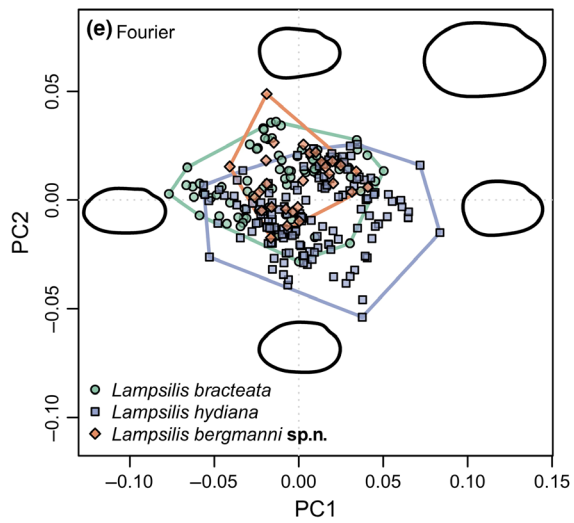
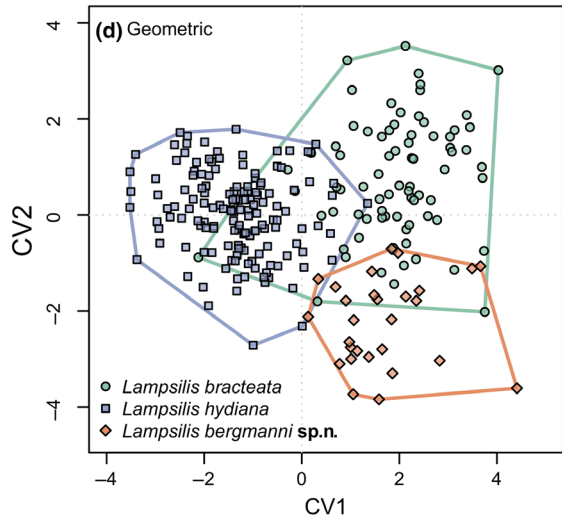
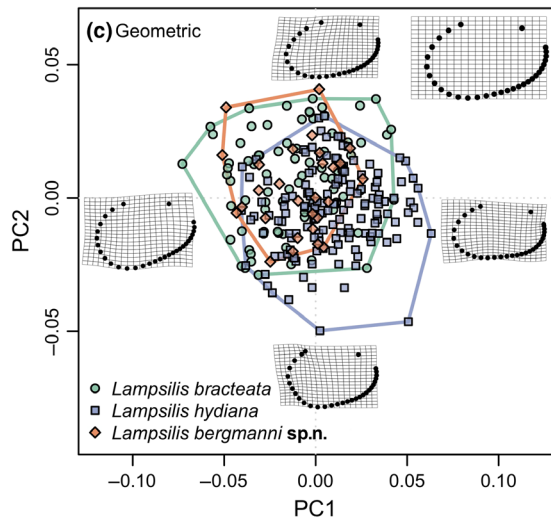
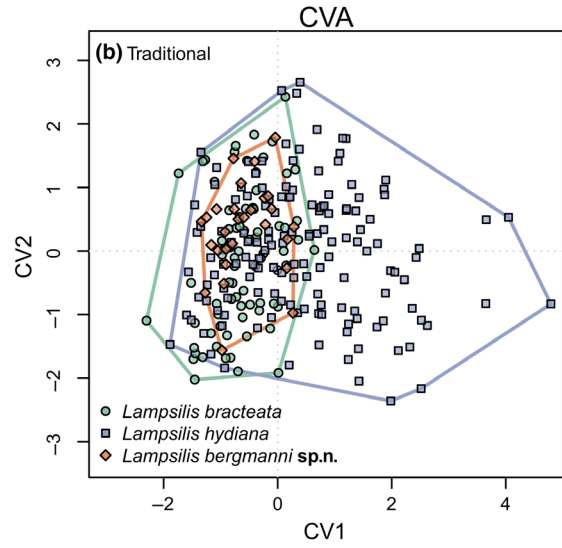
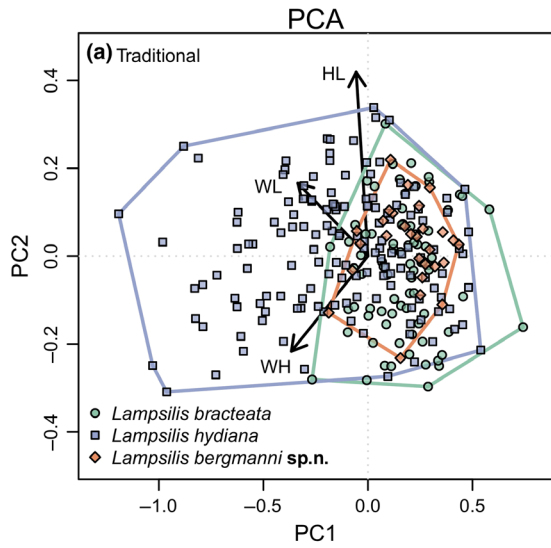


Table 3

Confusion matrix with percentages of individuals in *a priori* species classification (rows) that are assigned to the predicted species (columns) based on a discriminant function analysis for traditional, geometric and Fourier morphometrics. *A priori* species classification includes *Lampsilis bracteata*, *L. hydiana* and *L. bergmanni sp.n.*

	<i>Lampsilis bracteata</i>	<i>Lampsilis hydiana</i>	<i>Lampsilis bergmanni sp.n.</i>
Traditional morphometrics			
<i>Lampsilis bracteata</i>	51.9	35.4	12.7
<i>Lampsilis hydiana</i>	28.6	57.1	14.3
<i>Lampsilis bergmanni sp.n.</i>	20.5	22.6	56.8
Geometric morphometrics			
<i>Lampsilis bracteata</i>	84.8	10.1	5.1
<i>Lampsilis hydiana</i>	10.7	89.3	0
<i>Lampsilis bergmanni sp.n.</i>	4.1	2.7	93.2
Fourier morphometrics			
<i>Lampsilis bracteata</i>	89.9	5.1	5.1
<i>Lampsilis hydiana</i>	3.6	96.4	0
<i>Lampsilis bergmanni sp.n.</i>	2.7	0	97.3

Diagonal values for each morphometric analysis indicate a percentage of individuals in *a priori* species classification that are correctly predicted to be assigned to the species.

assignment of individuals to groups by DFA was 55.3% (range 51.9–57.1%; Table 3).

For geometric morphometrics, the PCA yielded five distinct eigenvalues that described > 90% of the total variation (Fig. 6c). The PC1 axis described 43% and the PC2 axis described 19% of the total variation. The PCA plot showed similar clustering patterns to the traditional morphometrics, where large portions of the clusters overlapped (Fig. 6c). However, CVA clusters showed significant differentiation among species (Fig. 6d). Similar to the traditional morphometrics, the MANOVA showed significant differences between mean shell morphologies of each species (Wilk's $\Lambda = 0.158$; $F_{124,378} = 4.6$; $P < 0.001$), except between *L. bracteata* and *L. cf. bracteata* ($P = 0.510$). Mean correct assignment of individuals to groups was 89.1% (range 84.8–93.2%; Table 3).

For Fourier morphometrics, the PCA yielded five distinct eigenvalues that described > 90% of the total variation (Fig. 6e). The PC1 axis described 59% and the PC2 axis described 20% of the total variation. The PCA plot showed similar clustering patterns to the traditional and geometric morphometrics (Fig. 6e). Similar to the geometric morphometrics, CVA clusters showed significant differentiation in shell morphologies among species (Fig. 6f). The MANOVA showed significant differences between species (Wilk's $\Lambda = 0.104$; $F_{154,348} = 4.8$; $P < 0.001$), except between *L. bracteata* and *L. cf. bracteata* ($P = 1$). Mean correct assignment of individuals to groups was 94.5% (range 89.9–97.3%; Table 3).

Soft anatomy characters

The arrangement of soft anatomy was similar among the species (Fig. 7). Soft tissues were generally

creamy white to slightly tan, and dark pigmentation was present on the posterior margin of the mantle tissue. *Lampsilis hydiana* had significantly larger, opaque white labial palps (Fig. 7b), whereas *L. bracteata* and *L. cf. bracteata* had smaller, translucent tan labial palps (Fig. 7a,c). Females had well-developed mantle flaps on the posterior margin of the mantle tissue and dark pigmentation on the posteroventral margin of outer gills accentuating the ovisacs (Fig. 7).

Incurrent and excurrent aperture papillae were heavily pigmented with orange-brown to dark grey, and their shape was slightly different among the species (Fig. 8). Incurrent aperture papillae were dark orange to brown in *L. bracteata* but lighter coloured in *L. hydiana*; however, *L. cf. bracteata* had pale orange papillae. In the incurrent aperture, *L. bracteata* had relatively short, stout and less dense simple papillae (Fig. 8a), whereas *L. hydiana* and *L. cf. bracteata* had long, slender and dense simple papillae (Fig. 8b,c). Some *L. hydiana* papillae were bifurcated (Fig. 8b). Excurrent aperture papillae were simple, short and less dense in *L. bracteata*; however, *L. hydiana* and *L. cf. bracteata* had relatively long and dense simple papillae (Fig. 8).

The MANOVA revealed significant differences in soft anatomical characters between species (Wilk's $\Lambda = 0.089$; $F_{22,62} = 6.6$; $P < 0.001$), except between *L. bracteata* and *L. cf. bracteata* ($P = 0.089$). The PCA yielded seven distinct eigenvalues that described > 90% of the total variation (Fig. 9). The PC1 axis described 25% and the PC2 axis described 21% of the total variation. The PCA plot showed significant clustering patterns grouped by species, where the *L. hydiana* cluster was differentiated from the other species (Fig. 9). A large portion of the *L. bracteata* and *L. cf. bracteata* clusters overlapped. The biplots

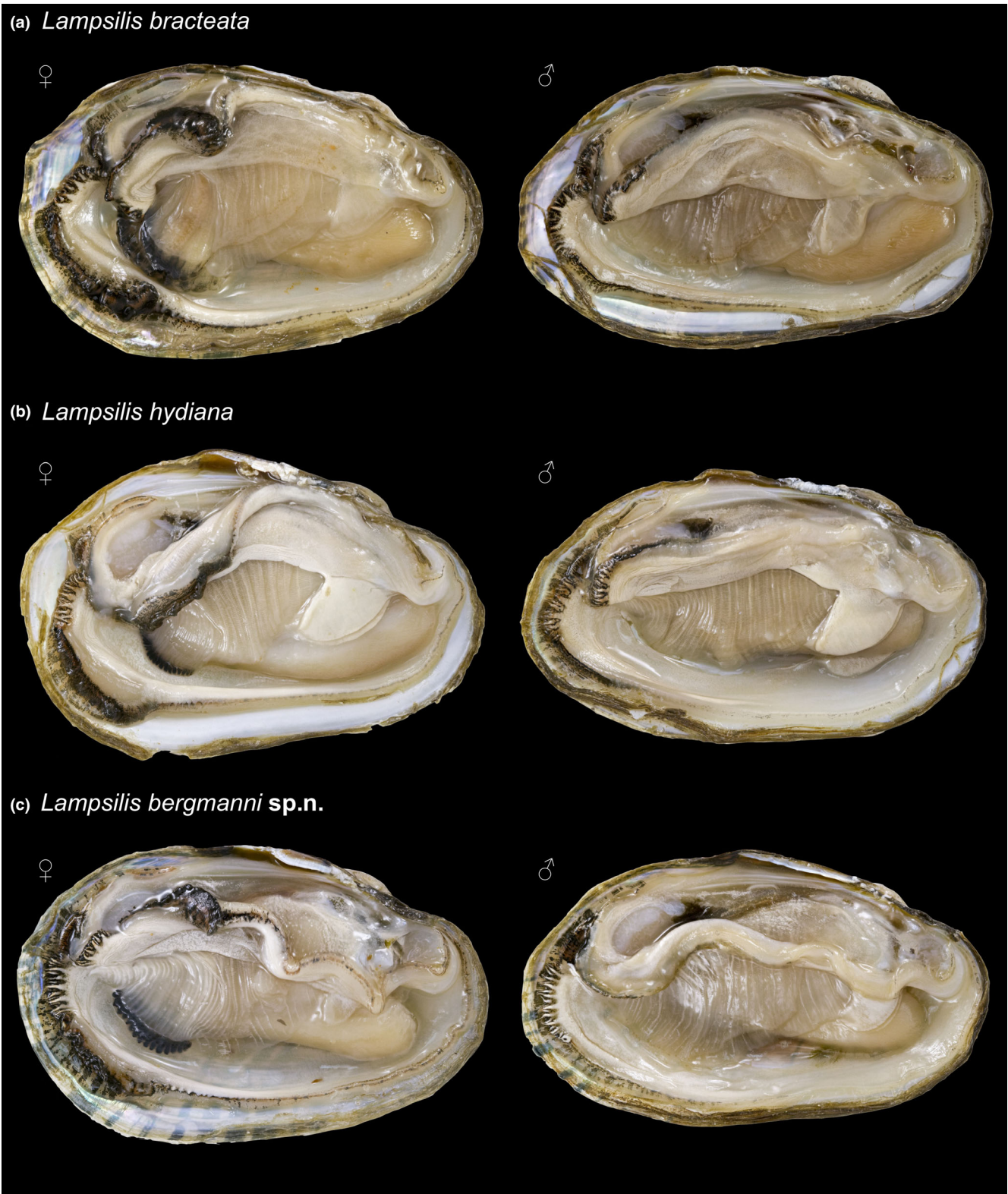


Fig. 7. Soft anatomy. (a) *Lampsilis bracteata*: female, 53.6 mm length (left); male, 62.7 mm length (right), San Saba River (Colorado River basin), Menard County, Texas. (b) *Lampsilis hydiana*: female, 61.0 mm length (left); male, 63.4 mm length (right), Cibolo Creek (San Antonio River basin), Wilson County, Texas. (c) *Lampsilis bergmanni* sp.n.: female, 57.0 mm length (left); male, 50.7 mm length (right), Guadalupe River, Kerr County, Texas.

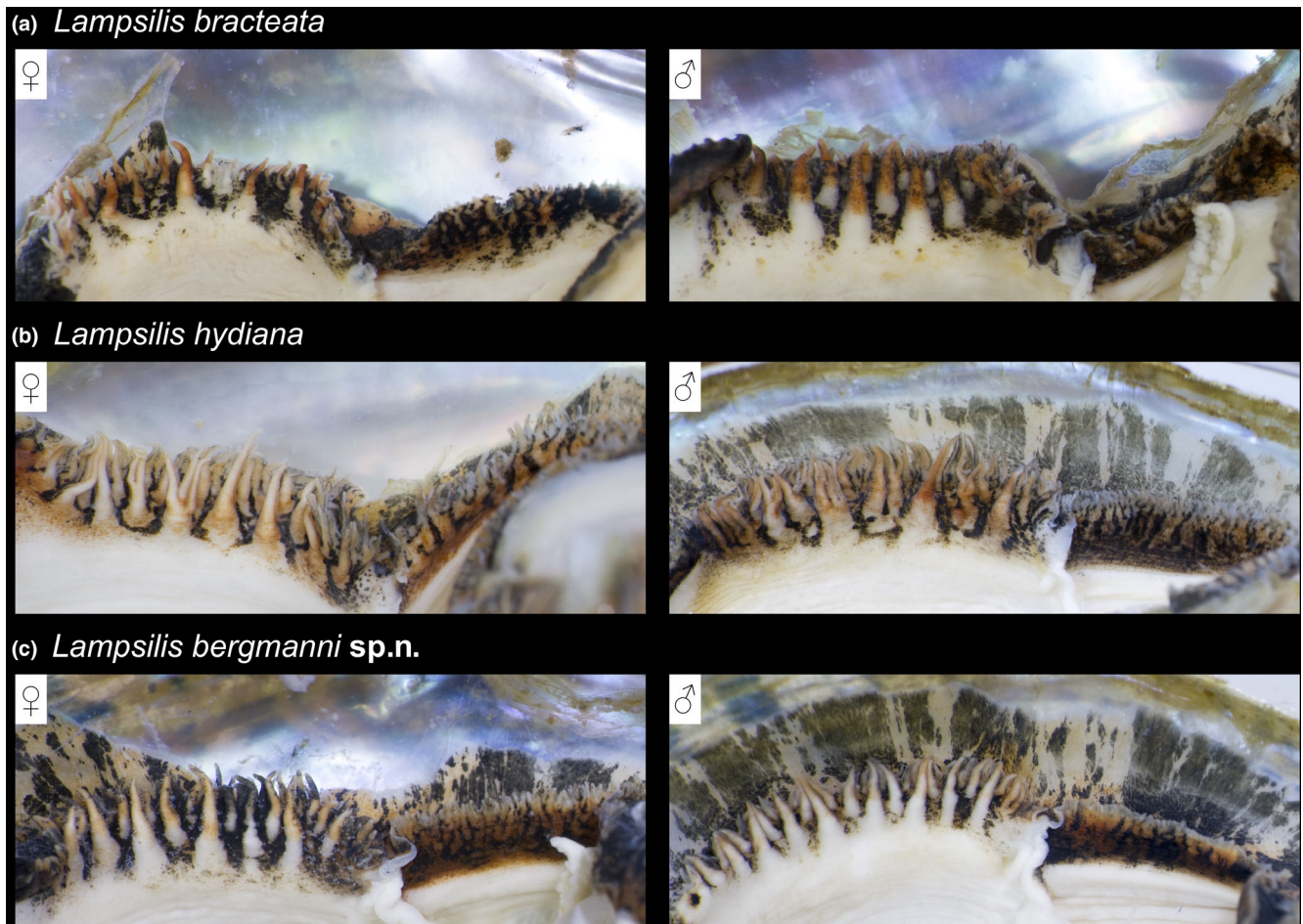


Fig. 8. Papillae of the incurrent and excurrent apertures. (a) *Lampsilis bracteata*: female (left), male (right), San Saba River (Colorado River basin), Menard County, Texas. (b) *Lampsilis hydiana*: female (left), male (right), Cibolo Creek (San Antonio River basin), Wilson County, Texas. (c) *Lampsilis bergmanni* sp.n.: female (left), male (right), Guadalupe River, Kerr County, Texas.

showed that labial palp length and height, inner gill height, incurrent aperture length and foot length were discriminant factors between *L. hydiana* and the other species (Fig. 9).

Taxonomic accounts

Based on the molecular, morphological and anatomical data, we herein describe *Lampsilis bergmanni* sp.n. from the upstream portion of the Guadalupe River and its tributaries of the Edwards Plateau, Texas, USA. A subset of the authors of the current study, Inoue and Randklev, are the authors of the new species. Specimens from the following institutions were examined in taxonomic accounts: Arkansas State University Museum of Zoology (ASUMZ), Baylor University Mayborn Museum (BV), Illinois Natural History Survey (INHS), Smithsonian Museum of Natural History (NMNH) and Texas A&M Natural Resources Institute Freshwater Mussel Collection (NRI).

Systematics

Class Bivalvia Linnaeus, 1758
 Order Unionida Gray, 1854
 Family Unionidae Rafinesque, 1820
 Genus *Lampsilis* Rafinesque, 1820

Lampsilis bergmanni Inoue and Randklev sp.n. (Figs 7c, 8c, 10, 11c, 12c and 13c). *Common name*. Guadalupe Fatmucket.

Range. Upstream portion of the Guadalupe River and its tributaries of the Edwards Plateau region in Kerr, Kendall and Comal counties, Texas, USA.

Type material. *Holotype*: INHS90608, Guadalupe River, upstream of Erhlers Road bridge, 5.2 air km SW of Comfort, Kerr County, Texas, 29.93975, -98.94837, 10.IV.2018, female, 57.0 mm length, *Allotype*: INHS90609, same data as holotype, male, 55.7 mm length. *Paratypes*: INHS90610 ($n = 10$), same data as holotype. NRI8512 ($n = 11$), same data as

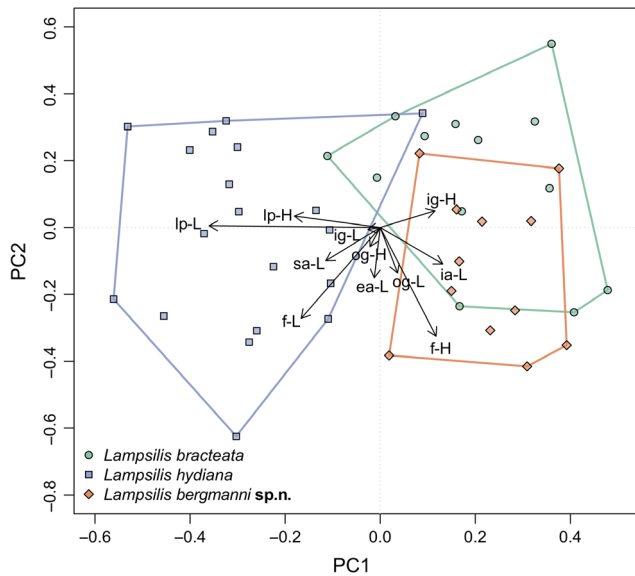


Fig. 9. Biplots from principal component analysis (PCA) of soft anatomical characters. Colours and shapes of points correspond to putative species (green circles, *Lampsilis bracteata*; blue squares, *L. hydiana*; orange diamonds, *L. bergmanni* sp.n.). Polygons enclose convex hulls of each species. Biplots of variables are shown in arrows. See Fig. 2 for abbreviations of soft anatomy characters. L, length; H, height.

holotype. NRI8308 ($n = 5$), Guadalupe River, downstream of Nimitz Lake, 2.3 air km WNW of Kerrville, Kerr County, Texas, 30.05230, -99.16366 , 14.III.2017. NRI8335 ($n = 9$), Guadalupe River, downstream of Nimitz Lake, 2.4 air km WNW of Kerrville, Kerr County, Texas, 30.05248, -99.16396 , 25.V.2017.

Material examined. NRI8697 ($n = 2$), Johnson Creek (Guadalupe River basin), Byas Springs Road bridge, 5.1 air km SE of Mountain Home, Kerr County, Texas, 30.146825, -99.338291 . BV197AB, BV198AB, Guadalupe River, New Braunfels, Comal County, Texas. BV2493AB, Guadalupe River, Kendall County, Texas. BV5243AB, Guadalupe River, Comfort, Kerr County, Texas.

Etymology. It is with honour that we name this species for Mr Joseph Anthony Michael Bergmann of Boerne, Texas, who dedicated much of his career (1970s to 2010s) to the collection and conservation of freshwater mussels in Texas and surrounding areas.

Comparative diagnosis. *Lampsilis bergmanni* sp.n. and *L. bracteata* are indistinguishable by conchological and soft anatomy morphologies; however, these species are not sympatric as each occurs within different river basins of the Edwards Plateau region. *Lampsilis bergmanni* sp.n. may resemble *L. hydiana*, but *L. bergmanni* sp.n. is more vividly rayed and has a thinner shell. Both species occur within the Guadalupe River basin; however, they are not syntopic. *Lampsilis bergmanni* sp.n. is restricted to the upstream portion of the

Guadalupe River and its tributaries of the Edwards Plateau, whereas *L. hydiana* ranges throughout the downstream portion of the Guadalupe River and adjacent tributaries of the Gulf Coastal Plain. *Lampsilis bergmanni* sp.n. is distinguished from *L. bracteata* and *L. hydiana* by one diagnostic nucleotide at *cox1* (289:G), one diagnostic nucleotide at *nad1* (240:C), two diagnostic nucleotides at *ITS1* (436:G, 473:G) and one diagnostic heterozygous locus at *ANT* (424:C/T).

Shell description. Shell length to *c.* 100 mm. Shell outline elliptical to quadrate or nearly ovate. Sexually dimorphic with male outline typically elliptical, female shape more oval or quadrate. Posterior margin pointed in males and broadly rounded to truncate in females. Posterior ridge rounded and scarcely perceptible. Shells thin but moderately solid and somewhat inflated, more so for females than males. Periostracum texture subglossy, tan to greenish-yellow base overlain with numerous brown or green rays that are wider at the shell margin and are often broken (Howells, 2014). Nacre white, usually iridescent posteriorly. Umbo broad and elevated above the hinge line, sculpture (when present) consisting of double-looped or v-shaped ridges. Umbo cavity typically shallow but can be moderately deep. Left valve with two thin lateral teeth, typically straight or slightly curved; two, triangular, compressed pseudocardinal teeth. Right valve with a single thin and long lateral tooth, and one compressed, triangular, often ragged edged pseudocardinal tooth, with an anterior denticle. Interdentum moderately long and thin.

Soft anatomy description. Mantle creamy white to light yellow. Aperture margins dark, often mottled with dark and light pigmented areas. Female with well-developed mantle flap, coloration black to dark orange, flap margin papillate, anterior margin enlarged into a tail-like structure. Males have a rudimentary flap, mottled with alternating dark and light areas. Incurrent and supra-anal apertures longer than excurrent aperture; incurrent aperture longer than supra-anal aperture. Incurrent aperture (length 12–16% of shell length) with dark grey to dark brown medial band on mantle, basal insertion of papillae creamy white to dark tan, free papillae stalks creamy white to orange, papillae elongate and tapered distally with simple tips, distal tips light grey to orange. Excurrent aperture (length 7–12% of shell length) with broad band of dark pigment internally, excurrent aperture papillae in single row and smaller than incurrent aperture papillae. Supra-anal aperture (length 7–17% of shell length) elongated and lacking papillae, supra-anal opening rimmed with dark grey to orange, often mottled with alternating dark and light areas. Gills creamy white to light tan. Female outer gill marsupial, posterior 1/3 to 1/2 utilized as ovisac, ovisac greatly distended, creamy white to light tan medially, dark grey

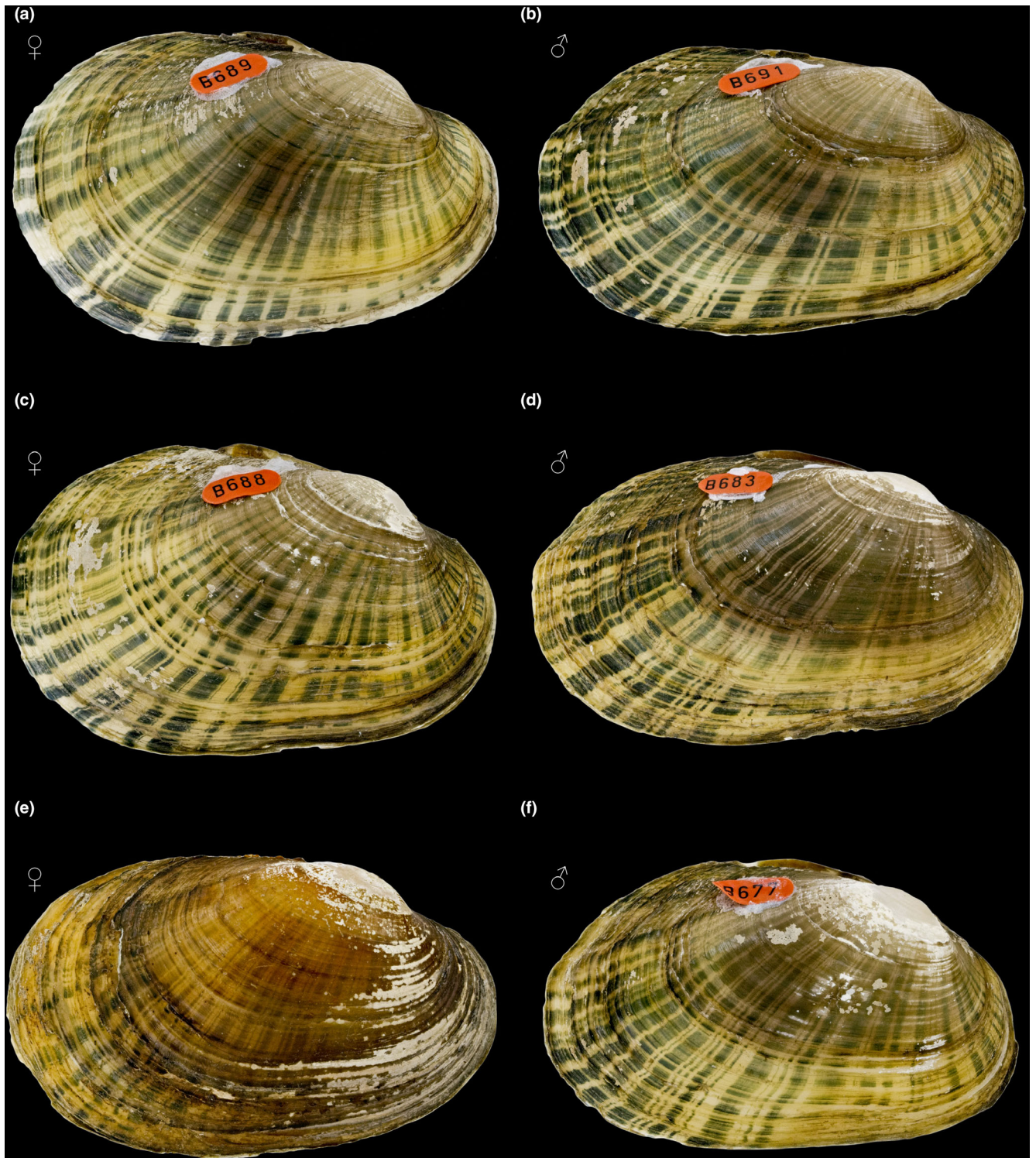


Fig. 10. Right valve of *Lampsilis bergmanni* sp.n. from the Guadalupe River, Kerr County, Texas. (a–f). (a) Holotype (INHS90608), female, 57.0 mm length; (b) allotype (INHS90609), male, 55.7 mm length; (c) paratype (NRI8512.15), female, 57.5 mm length; (d) paratype (INHS90610), male, 61.7 mm length; (e) paratype (NRI8335.3), female, 66.1 mm length; (f) paratype (INHS90610), male, 53.4 mm length. INHS, Illinois Natural History Survey; NRI, Texas A&M Natural Resources Institute Freshwater Mussel Collection.

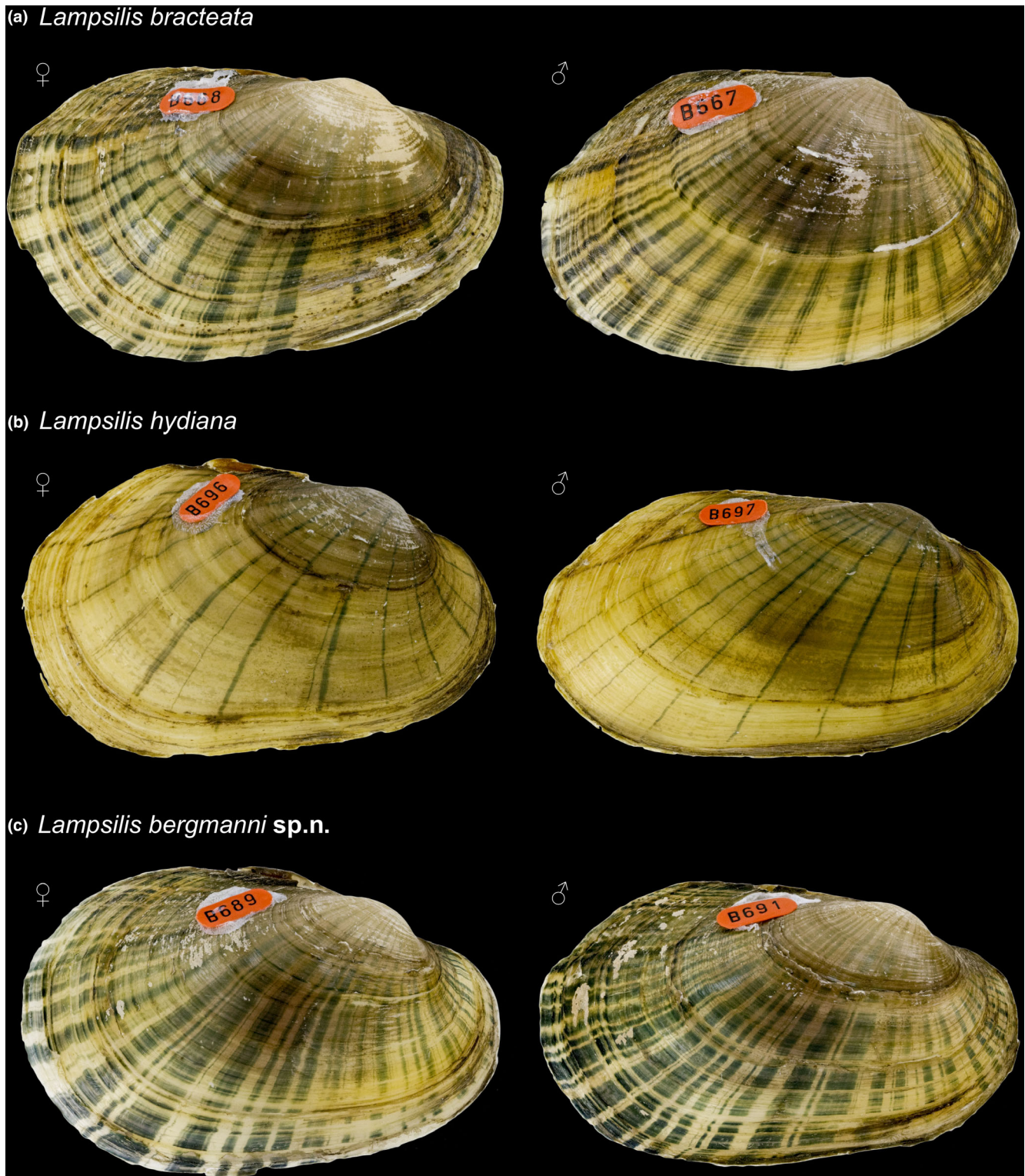


Fig. 11. Right valve external views. (a) *Lampsilis bracteata*: female, 59.6 mm length (left); male, 51.3 mm length (right), Cherokee Creek (Colorado River basin), San Saba County, Texas. (b) *Lampsilis hydiana*: female, 61.0 mm length (left); male, 65.0 mm length (right), Cibolo Creek (San Antonio River basin), Wilson County, Texas. (c) *Lampsilis bergmanni* sp.n.: female, 57.0 mm length (left); male, 55.7 mm length (right), Guadalupe River, Kerr County, Texas.

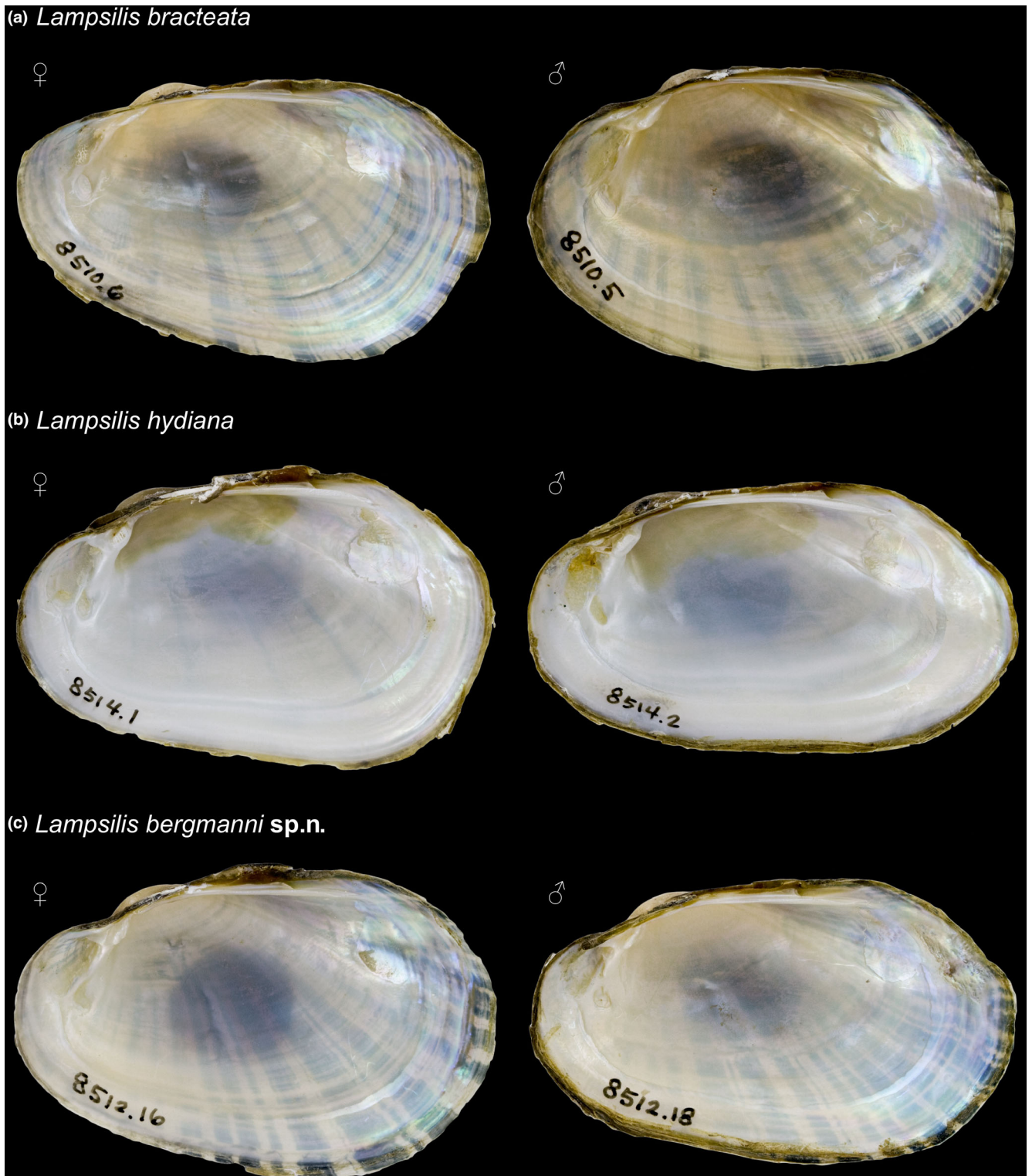


Fig. 12. Right valve internal views. (a) *Lampsilis bracteata*: female, 59.6 mm length (left); male, 51.3 mm length (right), Cherokee Creek (Colorado River basin), San Saba County, Texas. (b) *Lampsilis hydiana*: female, 61.0 mm length (left); male, 65.0 mm length (right), Cibolo Creek (San Antonio River basin), Wilson County, Texas. (c) *Lampsilis bergmanni* sp.n.: female, 57.0 mm length (left); male, 55.7 mm length (right), Guadalupe River, Kerr County, Texas.

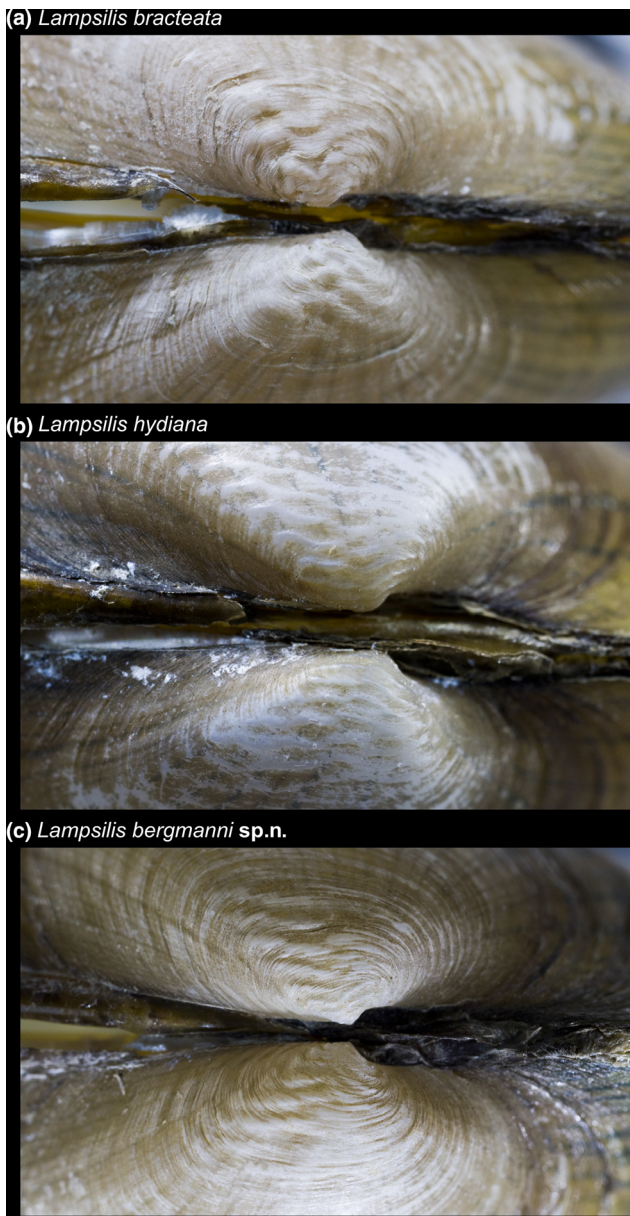


Fig. 13. . Umbo sculpture in (a) *Lampsilis bracteata*, (b) *Lampsilis hydiana* and (c) *Lampsilis bergmanni* sp.n.

to black on distal margin. Labial palps elongated (length:height = 1.3–2.0), colour creamy white to light tan, often translucent.

Remarks. *Lampsilis bergmanni* sp.n. does not have state or federal protection; however, this species is currently known from few localities. Studies are warranted to delineate the extent of the species distribution and evaluate the conservation status at state and federal levels.

Lampsilis bracteata (Gould, 1855) (Figs 7a, 8a, 11a, 12a and 13a). **Common name.** Texas Fatmucket.

Range. Major tributaries of the Colorado River basin within the Edwards Plateau region of Texas.

Type material. *Lectotype:* NMNH84966, designated by Johnson (1964:47, pl. 31, fig. 5), Llano River, near U.S. Highway 87, Mason County, Texas, examined by Taylor (1976).

Material examined. San Saba River: NRI8084 ($n = 1$), NRI8092 ($n = 5$), NRI8217 ($n = 2$), NRI8301 ($n = 20$ swab samples), NRI8302 ($n = 8$), NRI8436 ($n = 8$), NRI8440 ($n = 4$), NRI8523 ($n = 6$), San Saba River, 21.7 air km WSW of Menard, Menard County, Texas, 30.86759, –100.00657. Cherokee Creek: NRI8510 ($n = 11$), Cherokee Creek, 13.7 air km of ENE of Cherokee, San Saba County, Texas, 31.03243, –98.57802. Llano River: NRI8067 ($n = 1$), Hickory Creek, 14.7 air km WSW of Llano, Llano County, Texas, 30.71778, –98.82044; NRI8068 ($n = 2$), Llano River, 14.6 air km WSW of Llano, Llano County, Texas, 30.72080, –98.82051; NRI8267 ($n = 2$), South Llano River, 23.4 air km SW of Junction, Kimble County, Texas, 30.31681, –99.91180; NRI8273 ($n = 2$), James River, 35.5 air km E of Junction, Kimble County, Texas, 30.49734, –99.40220; NRI8275 ($n = 1$), Llano River, 1.6 air km E of Junction, Kimble County, Texas, 30.49227, –99.75590; NRI8276 ($n = 5$), North Llano River, 48.5 air km E of Sonora, Sutton County, Texas, 30.48279, –100.14739; NRI8286 ($n = 2$), Llano River, 27.8 air km W of Llano, Llano County, Texas, 30.70334, –98.95860; NRI8337 ($n = 11$), Llano River, 13.5 air km SW of Mason, Mason County, Texas, 30.65801, –99.32441. Pedernales River: NRI8087 ($n = 2$), Live Oak Creek, 5.5 air km SW of Fredericksburg, Gillespie County, Texas, 30.23939, –98.91184; NRI8306 ($n = 7$ swab samples), Pedernales River, 6.6 air km SSW of Fredericksburg, Gillespie County, Texas, 30.22282, –98.90490; NRI8307 ($n = 4$ swab samples), Pedernales River, 6.6 air km SSE of Fredericksburg, Gillespie County, Texas, 30.21864, –98.84947. Onion Creek: NRI8701 ($n = 1$ swab sample), Onion Creek, 15.3 air km ESE of Austin, Travis County, Texas, 30.20648, –97.59958; BV1089AB, BV1090AB, BV1091AB, BV1092AB, BV1093AB, BV1094AB, BV1095AB, BV1096AB, BV1097AB, BV1098AB, BV1099AB, BV1100AB, BV1101AB, BV1102AB, Onion Creek, 0.7 air km NW of Buda, Hays County, Texas, 30.08620, –97.84824.

Comparative diagnosis. *Lampsilis bracteata* and *L. bergmanni* sp.n. are indistinguishable morphologically; however, they are not sympatric as *L. bracteata* is endemic to the Colorado River basin and *L. bergmanni* sp.n. is endemic to the upper Guadalupe River basin. *Lampsilis bracteata* can be confused with *L. hydiana*; however, *L. hydiana* does not occur in the Colorado River basin. *Lampsilis bracteata* is distinguished from *L. bergmanni* sp.n. and *L. hydiana* by 46

diagnostic nucleotides at *cox1* (13:G, 16:G, 22:A, 29:G, 37:G, 43:T, 118:T, 127:A, 160:A, 169:G, 190:T, 211:A, 244:G, 256:A, 265:A, 268:G, 271:A, 286:G, 292:A, 295:G, 307:G, 325:T, 328:A, 331:A, 334:A, 343:C, 349:A, 355:A, 373:A, 457:T, 460:G, 466:A, 493:G, 520:T, 526:T, 535:G, 544:G, 545:G, 550:G, 559:A, 578:C, 580:G, 604:A, 607:A, 619:A, 649:G), 59 diagnostic nucleotides at *nad1* (8:A, 12:G, 15:A, 48:C, 53:T, 56:A, 68:C, 89:C, 122:G, 134:T, 143:C, 161:C, 182:G, 200:T, 210:C, 215:A, 218:T, 222:C, 235:C, 246:C, 257:G, 266:A, 281:C, 287:G, 290:C, 314:C, 320:T, 321:T, 323:A, 344:T, 353:C, 365:T, 371:T, 386:C, 401:T, 422:C, 428:C, 431:T, 437:C, 458:C, 461:C, 470:C, 471:C, 491:A, 507:G, 508:T, 509:A, 514:C, 515:C, 524:T, 530:C, 532:C, 533:C, 536:G, 551:C, 554:C, 563:A, 566:A, 569:T), seven diagnostic nucleotides at *ITS1* (56:C, 60:C, 81:T, 203:G, 242:A, 243:A, 438:C), and two diagnostic homozygous (424:C) and heterozygous (166:G/T) loci at *ANT*.

Shell description. Shell length to *c.* 100 mm. Shell outline elliptical, elongate-oval to quadrate. Sexually dimorphic, males more elliptical and females oval to quadrate. Posterior margin pointed to rounded in males, broadly rounded to truncate in females. Posterior ridge broadly rounded. Shells thin to slightly thick, moderately solid and moderately inflated, females often slightly more inflated than males. Periostracum texture subglossy, tan to greenish-yellow base overlain with numerous brown or green wavy rays that are wider at the margin and are often broken (Howells, 2014). Nacre usually white, iridescent posteriorly, sometimes with a salmon or yellowish tint. Umbo broad and elevated above the hinge line, sculpturing (when present) faint to prominent double-looped or v-shaped ridges. Umbo cavity shallow to moderately deep. Left valve with two thin lateral teeth, straight to slightly curved; two triangular, compressed pseudocardinal teeth. Right valve with single thin and relatively long lateral tooth, and one compressed triangular, often serrated pseudocardinal tooth; may have an anterior denticle. Interdentum moderately long and narrow.

Soft anatomy description. Mantle creamy white to light yellow. Aperture margins uniformly dark to sometimes mottled with dark and light pigmented areas. Females with well-developed mantle flap, coloration black to dark orange, flap margin papillate, anterior margin enlarged into a tail-like structure. Males with rudimentary flap, darker posteriorly, often mottled with alternating dark and light areas. Incurrent and supra-anal apertures similar in length; excurrent aperture shorter than incurrent and supra-anal apertures. Incurrent aperture (length 9–19% of shell length) with dark orange to dark brown medial band on mantle, basal insertion of papillae light or dark coloured, free papillae stalks black to orange, papillae elongated and tapered

distally with simple tips, light tan to dark orange. Excurrent aperture (length 6–10% of shell length) with broad dark band internally; excurrent aperture papillae in single row, smaller than incurrent aperture papillae. Supra-anal aperture (length 9–15% of shell length) elongate and lacking papillae; opening rimmed with black or dark grey pigment, sometimes mottled with alternating dark and light areas. Gills light to dark tan; female outer gill marsupial, posterior 1/2 utilized as ovisac, ovisac greatly distended, creamy white to tan medially, dark grey to black on distal margin. Labial palps short and round (length to height ratio = 1.2–1.8), colour light tan to yellow, often translucent.

Remarks. *Lampsilis bracteata* is listed as threatened by the state of Texas (TPWD, 2010) and is a candidate for listing under the U.S. Endangered Species Act (USFWS, 2009).

Lampsilis hydiana (Lea, 1838) (Figs 7b, 8b, 11b, 12b and 13b). *Common name.* Louisiana Fatmucket.

Range. The lower portion of the Mississippi Interior Basin and its major tributaries (St Francis, White, Ouachita and Red rivers) and western Gulf coastal rivers (the Mississippi River west to the Nueces River).

Type material. *Lectotype:* NMNH85010.

Verbatim type locality. “Teche River, Louisiana.”

Material examined. Ouachita River: NRI8079 (*n* = 1), Bayou Bartholomew, 19.3 air km NNE of Bastrop, Morehouse Parish, Louisiana, 32.92115, –91.80633; NRI8507 (*n* = 1), ASUMZ4573, ASUMZ4574, ASUMZ4638, ASUMZ4639, Irons Fork of the Ouachita River, 9.8 air km ENE of Mena, Polk County, Arkansas, 34.61667, –94.13928. Red River: NRI8120 (*n* = 2), Big Pine Creek, 29.5 air km NNW of Clarksville, Red River County, Texas, 33.86522, –95.14796; NRI8239 (*n* = 1), Little Cypress Bayou, 7.4 air km W of Woodlawn, Harrison County, Texas, 32.67222, –94.42500; NRI8562 (*n* = 4), Little River, 5.2 air km N of Idabel, McCurtain County, Oklahoma, 33.94060, –94.81160; NRI8570 (*n* = 1), Blue River, 1.1 air km N of Milburn, Johnston County, Oklahoma, 34.25089, –96.54951; NRI8684 (*n* = 2), Barkman Creek, 12.6 air km NW of Texarkana, Bowie County, Texas, 33.51062, –94.13741. Calcasieu River: NRI8694 (*n* = 2), Calcasieu River, 2.7 air km WSW of Oakdale, Allen Parish, Louisiana, 30.80733, –92.68476. Sabine River: NRI8111 (*n* = 4), Big Cow Creek, 9.6 air km NW of Newton, Newton County, Texas, 30.91904, –93.81649; NRI8114 (*n* = 1), Big Cow Creek, 4.3 air km SW of Newton, Newton County, Texas, 30.81886, –93.78563; NRI8117 (*n* = 2), Caney Creek, 11.8 air km SE of Newton, Newton County, Texas, 30.77585, –93.66767; NRI8130 (*n* = 1), Sabine River, 2.7 air km N of Deweyville, Newton County, Texas, 30.32133,

–93.75030; NRI8159 ($n = 4$), Sabine River, 10.2 air km WNW of Starks, Calcasieu Parish, Louisiana, 30.34050, –93.76383; NRI8347 ($n = 5$), Sabine River, 26.8 air km WSW of Singer, Beauregard Parish, Louisiana, 30.59268, –93.68238; NRI8352 ($n = 1$), NRI8393 ($n = 1$), Sabine River, 10.2 air km WNW of Starks, Calcasieu Parish, Louisiana, 30.34050, –93.76383; NRI8399 ($n = 4$), Sabine River, 9.17 air km W of Stark, Calcasieu Parish, Louisiana, 30.33145, –93.75581; NRI8417 ($n = 2$), Sabine River, 13.1 air km N of Deweyville, Newton County, Texas, 30.41543, –93.73332. Neches River: NRI8038 ($n = 1$), Neches River, 17.8 air km W of Kirbyville, Jasper County, Texas, 30.65901, –94.07868; NRI8051 ($n = 7$), Neches River, 15.3 air km W of Kirbyville, Tyler & Jasper Counties, Texas, 30.64316, –94.05171; NRI8155 ($n = 1$), Angelina River, 20.5 km SW of Nacogdoches, Nacogdoches County, Texas, 31.48693, –94.82360; NRI8311 ($n = 4$), NRI8319 ($n = 27$), Village Creek, 3.0 air km ESE of Lumberton, Hardin County, Texas, 30.25581, –94.17089; NRI8638 ($n = 13$), Village Creek, 2.3 air km NNE of Lumberton, Hardin County, Texas, 30.28505, –94.19161. Trinity River: NRI8467 ($n = 6$), Bedias Creek, 14.7 air km ESE of Madisonville, Madison County, Texas, 30.88456, –95.77792. San Jacinto River: NRI8029 ($n = 1$), NRI8464 ($n = 8$), East Fork of the San Jacinto River, 18.2 air km S of Coldspring, San Jacinto County, Texas, 30.42734, –95.12647; NRI8429 ($n = 3$), Lake Creek, 18.4 air km WSW of Conroe, Montgomery County, Texas, 30.24400, –95.63000. Brazos River: NRI8140 ($n = 1$), Navasota River, 2.7 air km W of Navasota, Grimes County, Texas, 30.38347, –96.13642; NRI8341 ($n = 13$), NRI8343 ($n = 9$), Navasota River, 9.4 air km WSW of Iola, Grimes County, Texas, 30.74558, –96.16711. Guadalupe River: NRI8164 ($n = 1$), NRI8360 ($n = 2$), NRI8435 ($n = 1$), Guadalupe River, 26.3 air km N of Cuero, Victoria County, Texas, 29.33077, –97.31154; NRI8700 ($n = 1$), San Marcos River, 13.1 air km NW of Gonzales, Gonzales County, Texas, 29.58969, –97.58514. San Antonio River: NRI8514 ($n = 6$), NRI8675 ($n = 15$), Cibolo Creek, 0.9 air km NNE of Sutherland Springs, Wilson County, Texas, 29.28090, –98.05413.

Comparative diagnosis. *Lampsilis bracteata* and *L. bergmanni* **sp.n.** have similar conchological characters to *L. hydiana*; however, *L. hydiana* tends to have a thicker shell and is less vividly rayed. These three species are not sympatric within their respective ranges. *Lampsilis hydiana* is distinguished from *L. bracteata* and *L. bergmanni* **sp.n.** by six diagnostic nucleotides at *cox1* (7:G, 110:C, 121:G, 253:A, 592:G, 625:G), two diagnostic nucleotides at *nad1* (92:G, 512:T) and two diagnostic homozygous loci at *ANT* (166:G, 424:C).

Shell description. Shell length to *c.* 125 mm (Howells, 2014), usually < 100 mm. Shell outline elliptical to quadrate. Sexually dimorphic, males more elliptical and females oval to quadrate. Posterior margin pointed in males, narrowly to broadly rounded in females, sometimes flattened and truncate. Posterior ridge flat to slightly curved and shells thin to moderately thick, solid and slightly inflated (males) to inflated (females). Periostracum texture subglossy, yellow, brown or olive, typically with broad to thin, continuous dark rays, occasionally absent or restricted to the posterior slope. Nacre white or iridescent, occasionally with blue-grey mottling. Umbo elevated slightly above hinge line, moderately full and high; sculpturing (when present) comprising double looped, parallel ridges. Umbo cavity shallow to moderately deep. Left valve with two, thin to moderately thick lateral teeth, straight to slightly curved, the ventral tooth often substantially larger; two, triangular compressed to thick pseudocardinal teeth. Right valve with a single thin, slightly curved, relatively long lateral tooth. One, compressed to large, triangular, blade-like or serrated pseudocardinal tooth; frequently with an enlarged anterior denticle often reported as a second pseudocardinal tooth. Interdentum long, about 1/2 the length of lateral teeth, and narrow.

Soft anatomy description. Mantle creamy white to light tan; aperture margins uniformly dark or banded with alternating dark and light pigmented areas. Females with well-developed mantle flap, coloration black to dark orange, flap margin papillate, anterior margin enlarged into a tail-like structure. Males with a rudimentary flap or flange bearing papillae, lighter coloured anteriorly progressing to a darker yellowish orange posteriorly. Supra-anal aperture usually longer than incurrent and excurrent apertures; incurrent aperture longer than excurrent aperture. Incurrent aperture (length 8–14% of shell length) with dark to very dark medial band on mantle, basal insertion of papillae lighter, free papillae stalks black to reddish brown, primary papillae (medial row) conical and elongate with simple or bifurcate tips, secondary papillae (distal row) elongate and simple or bifurcate, papillae distal tips often light grey. Excurrent aperture (length 7–11% of shell length) with broad band of dark pigment internally, excurrent aperture papillae in single row and smaller than incurrent aperture papillae. Supra-anal aperture (length 10–17% of shell length) elongate and lacking papillae, supra-anal opening rimmed with black or dark grey pigment, sometimes mottled with alternating dark and light areas. Gills light to dark tan. Female outer gill marsupial, posterior 1/3 to 1/2 utilized as ovisac, ovisac greatly distended, creamy white to tan medially, dark grey to black on distal margin. Labial palps elongated (length: height = 1.5–2.0), colour opaque creamy white, sometimes translucent.

Remarks. *Lampsilis hydiana* was considered stable throughout its range by Williams et al. (1993). Currently, *L. hydiana* is not of conservation concern and is not protected at the state or federal level.

Discussion

Our examination of *L. bracteata* and *L. hydiana* revealed that *L. bracteata* is not monophyletic but includes an undescribed species *L. bergmanni*. *Lampsilis bracteata* and *L. bergmanni* are genetically distinct from each other and did not form sister taxa. *Lampsilis bracteata* is a basal taxon of the *Bracteata* Lineage, whereas *L. bergmanni* is a member of the *Hydiana* Lineage. Despite the high genetic divergence between *L. bracteata* and *L. bergmanni*, we were unable to consistently differentiate the two using shell morphology or soft anatomy. Based on these data, we conclude that *L. bracteata* is restricted to tributaries of the Colorado River basin and *L. bergmanni* is endemic to the Guadalupe River basin upstream of New Braunfels, Texas.

We found that *L. bergmanni* is genetically distinct from *L. hydiana*, and formed a basal clade to *L. hydiana*, *L. straminea* and *L. virescens* in BI and ML trees. The genetic divergence is comparable to or greater than ones between other closely related mussel species (Jones et al., 2006b; Inoue et al., 2014; Pieri et al., 2018). Unlike our comparisons between *L. bracteata* and *L. bergmanni*, we found significant differences in shell morphology and soft anatomy between *L. bergmanni* and *L. hydiana*. Our *L. hydiana* samples included a wide geographical range from the Ouachita River to the San Antonio River; however, we did not observe phylogeographical structure within the species, suggesting the presence of active or recent gene flow between basins. Interestingly, *L. bergmanni* was genetically distinct from the Guadalupe River *L. hydiana*. We found genotypes for *L. bergmanni* only in the upstream reaches of the Guadalupe River and its tributaries, whereas *L. hydiana* genotypes were in the downstream portion of the Guadalupe River and its tributaries including the San Marcos River. Based on these results, *L. bergmanni* likely occurs only in portions of the Guadalupe River basin on the Edwards Plateau, above the Balcones fault line.

Within *Lampsilis*, phylogenetic relationships among species generally agree with current taxonomy. However, we found several groups of species requiring further taxonomic assessment. For example, our genetic results showed that *L. cardium* and *L. satura* were closely related and did not form reciprocally monophyletic clades. The distribution of *L. satura* is restricted to western Gulf coastal rivers (tributaries of the Red River west to the San Jacinto River; Vidrine,

1993; Howells, 2014), whereas *L. cardium* has a wide distributional range (Watters et al., 2009). However, the current study had small sample sizes and limited spatial coverage for these species. We recommend careful re-examination of these taxa before taxonomic revisions. Additionally, our results showed that *A. ligamentina* was nested within *Lampsilis* and sister to *L. higginsii*, which is congruent with previous studies (Chapman et al., 2008; Boyer et al., 2011). The validity of *Actinonaias* species in the USA and Canada has been questioned because of their disjunct distributions from the type species of the genus, *Actinonaias sapotalensis* (Lea, 1841) from the Río Papaloapan in Veracruz, Mexico (Williams et al., 2017). Further investigation that includes Mexican *Actinonaias* species is required to elucidate the generic assignment of species in the USA and Canada.

Forces driving speciation of the genus Lampsilis

Past geological events such as river capture and diversion are potentially key evolutionary forces for stream-dwelling taxa to expand their ranges and ultimately diversify their lineages (Hughes et al., 2009). Major diversifications within the genus *Lampsilis* occurred between the Oligocene and Pliocene epochs (30–2.5 Ma), where the *Bracteata* Lineage was separated from the *Hydiana* Lineage around the middle Oligocene. During the Paleocene to Eocene epochs (66.0–33.9 Ma), the ancestral Mississippi River basin had begun to develop river flow from the northern Rocky Mountains and northern margin of the Appalachian Mountains to the Gulf of Mexico (Galloway et al., 2011; Bentley et al., 2016). By the early Miocene epoch (~23 Ma), the Mississippi fluvial system established drainage patterns similar to the present-day Mississippi River and became one of the dominant sources of sediment to the Gulf of Mexico basin (Bentley et al., 2016). The initial diversification between the *Bracteata* and *Hydiana* Lineages corresponds to evolution of the Mississippi River in the middle Oligocene to early Miocene epochs, and species continued to diversify during the Miocene to Pliocene epochs. Given that both lineages are composed of species that are currently distributed widely in North America (i.e. from western Gulf of Mexico coastal rivers to Atlantic coastal rivers), the initial diversification of the lineages continued across the Mississippi River and its adjacent river basins during the Miocene and Pliocene epochs.

During the early Miocene, the Edwards Plateau of central Texas was elevated, which created the ancient Guadalupe and Colorado River basins that followed courses similar to their modern counterparts (Woodruff and Abbott, 1979; Galloway et al., 2011). The creation of these river basins in the Edwards Plateau likely isolated the ancestral *L. bracteata* lineage from

the rest of the *Bracteata* Lineage in the ancient Mississippi River. Similar isolations are predicted in other aquatic taxa, particularly in leuciscid fishes, in the Edwards Plateau and western Gulf coastal rivers (Richardson and Gold, 1995; Schonhuth and Mayden, 2010; Hoagstrom et al., 2013; Osborne et al., 2016). Consequently, rivers of the Edwards Plateau currently harbour a high number of endemic aquatic species, which evolved along with the formation of the plateau during the Miocene and Pliocene epochs. In contrast, *L. bergmanni*, which also is endemic to the Edwards Plateau, diversified from ancestral *L. hydiana* more recently—in the later Pliocene to the early Pleistocene epochs. Climate change and glaciation during this period caused fluctuating sea levels of the Gulf of Mexico, which led to stream capture events in this region (Woodruff, 1977). These climatic events, in turn, may have led to the diversification of *L. bergmanni* from *L. hydiana* and its isolation in the upstream portion of the Guadalupe River.

Hidden biodiversity in freshwater mussels

Recent molecular systematics of unionid mussels has identified cryptic species (Smith et al., 2017), refined taxonomy and systematics for various groups (Perkins et al., 2017; Pieri et al., 2018), and advanced our understanding of species diversity in freshwater mussels (Lopes-Lima et al., 2017; Inoue et al., 2018). Ecophenotypic plasticity in shell morphologies of freshwater mussels has been well-documented and can occur based on stream position and/or habitat (Utterback, 1917; Ortmann, 1920; Ball, 1922). This variation has caused taxonomic confusion, which resulted in the overestimation of species-level diversity (Inoue et al., 2013; Johnson et al., 2018). Because early taxonomists relied almost exclusively on morphological characters, > 4000 species have been described, of which ~840 species are currently recognized (Graf and Cummings, 2007). Three types of morphometrics analyses were used in the current study, and Fourier morphometrics outperformed the other methods. We were able to statistically differentiate *L. hydiana* from *L. bracteata* and *L. bergmanni*, but not between *L. bracteata* and *L. bergmanni*. The inability to statistically differentiate the two species morphologically explains why *L. bergmanni* has been long confused with *L. bracteata*. The similarity in morphology between the two species is likely in response to environmental conditions as both *L. bracteata* and *L. bergmanni* occur in small creeks and upstream reaches of medium-sized rivers; these species generally occur in substrates comprising sand, mud and gravel among large cobbles or in some cases within horizontal cracks in bedrock slabs (Howells, 2010). Utilizing molecular systematics, there will likely be more taxonomic changes

to come, particularly in understudied regions such as Mexico, Central and South America, and Asia (Boltov et al., 2017; Pfeiffer et al., 2018; Huang et al., 2019). The current study reiterates the importance of conducting molecular systematic studies and provides an example of underestimating the species diversity of freshwater mussels.

Implication for conservation

At its core, species conservation relies on the ability of biologists and their stakeholders to distinguish one species from another (Johnson et al., 2018). The results of this study indicate the presence of undescribed cryptic diversity within the *Hydiana* Lineage of *Lampsilis*, which has important conservation implications. First, the geographical range of *L. bracteata* is now reduced, comprising only a few tributaries of the Colorado River, all of which are generally reliant on spring and groundwater inputs to maintain base flows. Excessive water extraction in parts of the Edwards Plateau poses a significant challenge to maintenance of base flows and will likely impact the long-term persistence of *L. bracteata*, resulting in further reductions in its geographical distribution within this region. A recent study in the San Saba River, a tributary of the Colorado River on the Edwards Plateau, found that stream intermittency caused by excessive groundwater pumping has reduced the range of *L. bracteata* in the river (Randklev et al., 2018). For *L. bracteata* populations, we did not observe significant phylogeographic structure at mtDNA and nDNA sequence levels, indicating currently active or relatively recent gene flow among populations. However, given its current sporadic and restricted distribution due to anthropogenic factors, genetic markers used in the study might not detect recent diversification of populations. Additional population genetics studies using variable genetic markers (e.g. microsatellites or restriction-site associated DNA (RAD)) are warranted to understand fine-scale population genetic structure and genetic connectivity among populations. Such information is useful in future recovery efforts that may include captive propagation, augmentation and reintroduction (Jones et al., 2006a; McMurray and Roe, 2017). Furthermore, our findings indicate that *L. bergmanni* has a restricted distribution limited to upstream reaches of the Guadalupe River and its tributaries west of the Balcones fault line. The range of *L. bergmanni* likely has been severely reduced by the construction of Canyon Lake and several run-of-the-river reservoirs that in all probably eliminated large swaths of habitat for the species. Currently, *L. bergmanni* can be found at a number of locations throughout the range, most of which have low abundance. Based on its overall restricted distribution and limited number of known populations,

L. bergmanni warrants evaluation for listing at both the state and federal levels.

Acknowledgements

We thank M. Hart, J. Khan, S. Robertson, M. Fisher, A. Blair, S. Kinney, B. Gregory, K. Roe, S. Oetker, G. Pandolfi, J. Lewis, E. Orsak, C. Stevens, A. Seagroves and L. Johnston for collecting samples, and A. Pieri for help with molecular analyses. We also thank Kevin Cummings for discussion on *Actinonaias* in Mexico. Funding was provided by the Texas Parks and Wildlife Department and the U.S. Fish and Wildlife Service. Museum specimens were provided by: North Carolina State Museum of Natural Science (A. Bogan), Baylor University Mayborn Museum (A. Benedict) and Arkansas State University Museum of Zoology. Any use of trade, firm or product names is for descriptive purposes only and does not imply endorsement by the U.S. Government. Two anonymous reviewers provided insightful comments and greatly improved the quality and clarity of the final manuscript.

Conflict of interest

The authors declare no conflict of interest.

References

- Albert, J.S., Craig, J.M., Tagliacollo, V.A., Petry, P., 2018. Upland and lowland fishes: a test of the river capture hypothesis. In: Hoorn, C., Perrigo, A., Antonelli, A. (Eds.), *Mountains, Climate and Biodiversity*. John Wiley & Sons, Inc., Hoboken, NJ, pp. 273–294.
- Audzijonyte, A., Vrijenhoek, R.C., 2010. Three nuclear genes for phylogenetic, SNP and population genetic studies of molluscs and other invertebrates. *Mol. Ecol. Resour.* 10, 200–204.
- Avise, J.C., 2000. *Phylogeography: The History and Formation of Species*. Harvard University Press, Cambridge, MA.
- Ball, G.H., 1922. Variation in fresh-water mussels. *Ecology* 3, 93–121.
- Bentley, S.J., Blum, M.D., Maloney, J., Pond, L., Paulsell, R., 2016. The Mississippi River source-to-sink system: perspectives on tectonic, climatic, and anthropogenic influences, Miocene to Anthropocene. *Earth Sci. Rev.* 153, 139–174.
- Bolotov, I.N., Vikhrev, I.V., Bepalaya, Y.V., Gofarov, M.Y., Kondakov, A.V., Konopleva, E.S., Bolotov, N.N., Lyubas, A.A., 2016. Multi-locus fossil-calibrated phylogeny, biogeography and a subgeneric revision of the Margaritiferidae (Mollusca: Bivalvia: Unionoida). *Mol. Phylogenet. Evol.* 103, 104–121.
- Bolotov, I.N., Vikhrev, I.V., Kondakov, A.V., Konopleva, E.S., Gofarov, M.Y., Aksenova, O.V., Tumpeesuwan, S., 2017. New taxa of freshwater mussels (Unionidae) from a species-rich but overlooked evolutionary hotspot in Southeast Asia. *Sci. Rep.* 7, 11573.
- Bouckaert, R., Heled, J., Kühnert, D., Tim, V., Wu, C.-H., Xie, D., Suchard, M.A., Rambaut, A., Drummond, A.J., 2014. BEAST 2: a software platform for Bayesian evolutionary analysis. *PLoS Comput. Biol.* 10, e1003537.
- Bowles, D.E., Arsuffi, T.L., 1993. Karst aquatic ecosystems of the Edwards Plateau region of central Texas, USA: a consideration of their importance, threats to their existence, and efforts for their conservation. *Aquat. Conserv.* 3, 317–329.
- Boyer, S.L., Howe, A.A., Juergens, N.W., Hove, M.C., 2011. A DNA-barcoding approach to identifying juvenile freshwater mussels (Bivalvia: Unionidae) recovered from naturally infested fishes. *J. N. Am. Benthol. Soc.* 30, 182–194.
- Bromham, L., Penny, D., 2003. The modern molecular clock. *Nat. Rev. Genet.* 4, 216–224.
- Campbell, D.C., Serb, J.M., Buhay, J.E., Roe, K.J., Minton, R.L., Lydeard, C., 2005. Phylogeny of North American amblemines (Bivalvia: Unionoida): prodigious polyphyly proves pervasive across genera. *Invertebr. Biol.* 124, 131–164.
- Chapman, E.G., Gordon, M.E., Walker, J.M., Lang, B.K., Campbell, D., Watters, G.T., Curolé, J.P., Piontkivska, H., Hoeh, W.R., 2008. Evolutionary relationships of *Popenaias popeii* and the early evolution of lampsiline bivalves (Unionidae): phylogenetic analyses of DNA and amino acid sequences from F and M mitochondrial genomes. *Malacologia* 50, 303–318.
- Ezard, T., Fujisawa, T., Barraclough, T., 2013. R package splits: Species' Limits by Threshold Statistics, version 1.0. Available at: <https://r-forge.r-project.org/projects/splits/>
- Folmer, O., Black, M., Hoeh, W.R., Lutz, R., Vrijenhoek, R., 1994. DNA primers for amplification of mitochondrial cytochrome *c* oxidase subunit I from diverse metazoan invertebrates. *Mol. Mar. Biol. Biotechnol.* 3, 294–299.
- Froufe, E., Gonçalves, D.V., Teixeira, A., Sousa, R., Varandas, S., Ghamizi, M., Zieritz, A., Lopes-Lima, M., 2016. Who lives where? Molecular and morphometric analyses clarify which *Unio* species (Unionida, Mollusca) inhabit the southwestern Palearctic. *Org. Divers. Evol.* 16, 597–611.
- Galloway, W.E., Whiteaker, T.L., Ganey-Curry, P., 2011. History of Cenozoic North American drainage basin evolution, sediment yield, and accumulation in the Gulf of Mexico basin. *Geosphere* 7, 938–973.
- Gould, A.A., 1855. [Description of new shells]. *Proc. Boston Soc. Nat. Hist.* 5, 228–229.
- Graf, D.L., Cummings, K.S., 2007. Review of the systematics and global diversity of freshwater mussel species (Bivalvia: Unionoida). *J. Mollus. Stud.* 73, 291–314.
- Haag, W.R., 2010. A hierarchical classification of freshwater mussel diversity in North America. *J. Biogeogr.* 37, 12–26.
- Hammer, Ø., Harper, D.A.T., Ryan, P.D., 2001. PAST: paleontological statistics software package for education and data analysis. *Palaeontol. Electronica* 4, 1–9.
- Harris, J.L., Posey, W.R. II, Davidson, C.L., Farris, J.L., Oetker, S.R., Stoeckel, J.N., Crump, B.G., Barnett, M.S., Martin, H.M., Matthews, M.W. et al., 2010. Unionoida (Mollusca: Margaritiferidae, Unionidae) in Arkansas, third status review. *J. Ark. Acad. Sci.* 63, 50–86.
- Helaers, R., Milinkovitch, M.C., 2010. MetaPIGA v2.0: maximum likelihood large phylogeny estimation using the metapopulation genetic algorithm and other stochastic heuristics. *BMC Bioinformatics* 11, 379.
- Hewitt, G., 2000. The genetic legacy of the Quaternary ice ages. *Nature* 405, 907–913.
- Hoagstrom, C.W., Ung, V., Taylor, K., Ebach, M., 2013. Miocene rivers and taxon cycles clarify the comparative biogeography of North American highland fishes. *J. Biogeogr.* 41, 644–658.
- Hoang, D.T., Vinh, L.S., Flouri, T., Stamatakis, A., von Haeseler, A., Minh, B.Q., 2018. MPBoot: fast phylogenetic maximum parsimony tree inference and bootstrap approximation. *BMC Evol. Biol.* 18, 11.
- Howells, R.G., 2010. Freshwater mussels of Texas and the western Gulf Coast. *Freshwater Mollusk Conservation Society 2010 Workshop: Regional Fauna Identification and Sampling*, Kirkwood, MO, pp. 161–174.
- Howells, R.G. 2014. *Field Guide to Texas Freshwater Mussels*. BioStudies, Kerville, TX.

- Howells, R.G., Neck, R.W., Murray, H.D. 1996. Freshwater Mussels of Texas. Texas Park and Wildlife Department, Austin, TX.
- Huang, X.C., Su, J.H., Ouyang, J.X., Ouyang, S., Zhou, C.H., Wu, X.P., 2019. Towards a global phylogeny of freshwater mussels (Bivalvia: Unionida): species delimitation of Chinese taxa, mitochondrial phylogenomics, and diversification patterns. *Mol. Phylogenet. Evol.* 130, 45–59.
- Hughes, J.M., Schmidt, D.J., Finn, D.S., 2009. Genes in streams: using DNA to understand the movement of freshwater fauna and their riverine habitat. *Bioscience* 59, 573–583.
- Inoue, K., Hayes, D.M., Harris, J.L., Christian, A.D., 2013. Phylogenetic and morphometric analyses reveal ecophenotypic plasticity in freshwater mussels *Obovaria jacksoniana* and *Villosa arkansasensis* (Bivalvia: Unionidae). *Ecol. Evol.* 3, 2670–2683.
- Inoue, K., McQueen, A.L., Harris, J.L., Berg, D.J., 2014. Molecular phylogenetics and morphological variation reveal recent speciation in freshwater mussels of the genera *Arcidens* and *Arkansia* (Bivalvia: Unionidae). *Biol. J. Linnean Soc.* 112, 535–545.
- Inoue, K., Hayes, D.M., Harris, J.L., Johnson, N.A., Morrison, C.L., Eackles, M.S., King, T.L., Jones, J.W., Hallerman, E.M., Christian, A.D. et al., 2018. The Pleurobemini (Bivalvia: Unionida) revisited: molecular species delineation using a mitochondrial DNA gene reveals multiple conspecifics and undescribed species. *Invertebr. Syst.* 32, 689–702.
- Iwata, H., Ukai, Y., 2002. SHAPE: a computer program package for quantitative evaluation of biological shapes based on elliptic Fourier descriptors. *J. Hered.* 93, 384–385.
- Johnson, R.I., 1964. The recent Mollusca of Augustus Addison Gould. *Bull. U. S. Natl. Mus.* 239, 1–182.
- Johnson, N.A., Smith, C.H., Pfeiffer, J.M., Randklev, C.R., Williams, J.D., Austin, J.D., 2018. Integrative taxonomy resolves taxonomic uncertainty for freshwater mussels being considered for protection under the U.S. Endangered Species Act. *Sci. Rep.* 8, 15892.
- Jones, J.W., Hallerman, E.M., Neves, R.J., 2006a. Genetic management guidelines for captive propagation of freshwater mussels (Unionoidea). *J. Shellfish Res.* 25, 527–535.
- Jones, J.W., Neves, R.J., Ahlstedt, S.A., Hallerman, E.M., 2006b. A holistic approach to taxonomic evaluation of two closely related endangered freshwater mussel species, the Oyster Mussel *Epioblasma capsaeformis* and Tan Riffleshell *Epioblasma florentina walkeri* (Bivalvia: Unionidae). *J. Mollus. Stud.* 72, 267–283.
- Katoh, K., Standley, D.M., 2013. MAFFT multiple sequence alignment software version7: improvements in performance and usability. *Mol. Biol. Evol.* 30, 772–780.
- King, T.L., Eackles, M.S., Gjetvaj, B., Hoeh, W.R., 1999. Intraspecific phylogeography of *Lasmigona subviridis* (Bivalvia: Unionidae): conservation implications of range discontinuity. *Mol. Ecol.* 9, S65–S78.
- Kumar, S., Stecher, G., Tamura, K., 2016. MEGA7: Molecular Evolutionary Genetics Analysis version 7.0 for bigger datasets. *Mol. Biol. Evol.* 33, 1870–1874.
- Librado, P., Rozas, J., 2009. DnaSP v5: a software for comprehensive analysis of DNA polymorphism data. *Bioinformatics* 25, 1451–1452.
- Lopes-Lima, M., Froufe, E., Do, V.T., Ghamizi, M., Mock, K.E., Kebapci, U., Klishko, O., Kovitvadhi, S., Kovitvadhi, U., Paulo, O.S. et al., 2017. Phylogeny of the most species-rich freshwater bivalve family (Bivalvia: Unionida: Unionidae): defining modern subfamilies and tribes. *Mol. Phylogenet. Evol.* 106, 174–191.
- McMurray, S.E., Roe, K.J., 2017. Perspectives on the controlled propagation, augmentation, and reintroduction of freshwater mussels (Mollusca: Bivalvia: Unionoidea). *Freshw. Mollusk Biol. Conserv.* 20, 1–12.
- Minh, B.Q., Nguyen, M.A., von Haeseler, A., 2013. Ultrafast approximation for phylogenetic bootstrap. *Mol. Biol. Evol.* 30, 1188–1195.
- Neck, R.W. 1982. Preliminary analysis of the ecological zoogeography of the freshwater mussels of Texas. In: Davis, J.R. (Ed.) *Proceedings of the Symposium on Recent Benthological Investigations in Texas and Adjacent States*. Texas Academy of Science, Austin, TX, pp. 33–42.
- Ortmann, A.E., 1920. Correlation of shape and station in freshwater mussels (Naiades). *Proc. Am. Philos. Soc.* 59, 268–312.
- Osborne, M.J., Diver, T.A., Hoagstrom, C.W., Turner, T.F., 2016. Biogeography of ‘*Cyprinella lutrensis*’: intensive genetic sampling from the Pecos River ‘melting pot’ reveals a dynamic history and phylogenetic complexity. *Biol. J. Linnean Soc.* 117, 264–284.
- Perkins, M.A., Johnson, N.A., Gangloff, M.M., 2017. Molecular systematics of the critically-endangered North American spiny mussels (Unionidae: *Elliptio* and *Pleurobema*) and description of *Parvaspina* gen. nov. *Conserv. Genet.* 18, 745–757.
- Pfeiffer, J.M., Sharpe, A.E., Johnson, N.A., Emery, K.F., Page, L.M., 2018. Molecular phylogeny of the Nearctic and Mesoamerican freshwater mussel genus *Megaloniais*. *Hydrobiologia* 811, 139–151.
- Pieri, A.M., Inoue, K., Johnson, N.A., Smith, C.H., Harris, J.L., Robertson, C., Randklev, C.R., 2018. Molecular and morphometric analyses reveal cryptic diversity within freshwater mussels (Bivalvia: Unionidae) of the western Gulf coastal drainages of the USA. *Biol. J. Linnean Soc.* 124, 261–277.
- Pons, J., Barraclough, T., Gomez-Zurita, J., Cardoso, A., Duran, D., Hazell, S., Kamoun, S., Sulmlin, W., Vogler, A., 2006. Sequence-based species delimitation for the DNA taxonomy of undescribed insects. *Syst. Biol.* 55, 595–609.
- Rambaut, A., Drummond, A.J., Xie, D., Baele, G., Suchard, M.A., 2018. Posterior summarisation in Bayesian phylogenetics using Tracer 1.7. *Syst. Biol.* 67, 901–904.
- Randklev, C.R., Johnson, N.A., Miller, T., Morton, J., Dudding, J., Skow, K., Boseman, B., Hart, M., Tsakiris, E.T., Inoue, K. et al., 2017. *Freshwater Mussels (Unionidae): Central and West Texas Final Report*. Texas A&M Institute of Renewable Natural Resources, College Station, TX, pp. 312.
- Randklev, C.R., Tsakiris, E.T., Johnson, M.S., Popejoy, T., Hart, M.A., Khan, J., Geeslin, D., Robertson, C.R., 2018. The effect of dewatering on freshwater mussel (Unionidae) community structure and the implications for conservation and water policy: a case study from a spring-fed stream in the southwestern United States. *Glob. Ecol. Conserv.* 16, e00456.
- Reid, N.M., Carstens, B.C., 2012. Phylogenetic estimation error can decrease the accuracy of species delimitation: a Bayesian implementation of the general mixed Yule-coalescent model. *BMC Evol. Biol.* 12, 196.
- Richardson, L.R., Gold, J.R., 1995. Evolution of the *Cyprinella lutrensis* species group. III. Geographic variation in the mitochondrial DNA of *Cyprinella lutrensis*—the influence of Pleistocene glaciation on population dispersal and divergence. *Mol. Ecol.* 4, 163–171.
- Rohlf, F.J., 2018. tpsDIG32, tpsRelw. Software distributed by the author. Available at: <http://life.bio.sunysb.edu/morph/>.
- Ronquist, F., Teslenko, M., van der Mark, P., Ayres, D.L., Darling, A., Höhna, S., Larget, B., Liu, L., Suchard, M.A., Huelsenbeck, J.P., 2012. MrBayes 3.2: efficient Bayesian phylogenetic inference and model choice across a large model space. *Syst. Biol.* 61, 539–542.
- Saghai-Marooif, M.A., Soliman, K.M., Jorgensen, R.A., Allard, R.W., 1984. Ribosomal DNA spacer-length polymorphisms in barley: Mendelian inheritance, chromosomal location, and population dynamics. *Proc. Natl. Acad. Sci. USA* 81, 8014–8018.
- Schonhuth, S., Mayden, R.L., 2010. Phylogenetic relationships in the genus *Cyprinella* (Actinopterygii: Cyprinidae) based on mitochondrial and nuclear gene sequences. *Mol. Phylogenet. Evol.* 55, 77–98.
- Smith, C.H., Johnson, N.A., Pfeiffer, J.M., Gangloff, M.M., 2017. Molecular and morphological data reveal non-monophyly and speciation in imperiled freshwater mussels (*Anodontoidea* and *Strophitus*). *Mol. Phylogenet. Evol.* 119, 50–62.

- Strecker, J.K., 1931. The distribution of the naiades or pearly freshwater mussels of Texas. Baylor University Museum, Special Bulletin Number 2, pp. 1–71.
- Tanabe, A.S., 2011. Kakusan4 and Aminosan: two programs for comparing nonpartitioned, proportional and separate models for combined molecular phylogenetic analyses of multilocus sequence data. *Mol. Ecol. Resour.* 11, 914–921.
- Taylor, D.W., 1976. Freshwater mollusks collected by the United States and Mexican boundary surveys. *Veliger* 10, 152–158.
- TPWD, 2010. Threatened and endangered nongame species. Chapter 65. Wildlife Subchapter G. 31 TAC §65.175. Adopted rules. *Texas Regist.* 35, 249–251.
- Trifinopoulos, J., Nguyen, L.T., von Haeseler, A., Minh, B.Q., 2016. W-IQ-TREE: a fast online phylogenetic tool for maximum likelihood analysis. *Nucleic Acids Res.* 44, W232–W235.
- USFWS, 2009. Endangered and threatened wildlife and plants; 90-day finding on petitions to list nine species of mussels from Texas as threatened or endangered with critical habitat; proposed rule. *Fed. Regist.* 74, 66260–66271.
- Utterback, W.I., 1917. Naiadogeography of Missouri. *Am. Midl. Nat.* 5, 26–30.
- Vaughn, C.C., Mather, C.M., Pyron, M., Mehlhop, P., Miller, E.K., 1996. The current and historical mussel fauna of the Kiamichi River, Oklahoma. *Southwest. Nat.* 41, 325–328.
- Vidrine, M.F., 1993. The Historical Distributions of Freshwater Mussels in Louisiana. Gail Q. Vidrine Collectibles, Eunice, LA.
- Watters, G.T., Hoggarth, M.A., Stansbery, D.H., 2009. The Freshwater Mussels of Ohio. Ohio State University, Columbus, OH.
- Williams, J.D., Warren, M.L. Jr., Cummings, K.S., Harris, J.L., Neves, R.J., 1993. Conservation status of freshwater mussels of the United States and Canada. *Fisheries* 18, 6–22.
- Williams, J.D., Bogan, A.E., Garner, J.T., 2008. Freshwater Mussels of Alabama and the Mobile Basin in Georgia, Mississippi & Tennessee. The University of Alabama Press, Tuscaloosa, AL.
- Williams, J.D., Bogan, A.E., Butler, R.S., Cummings, K.S., Garner, J.T., Harris, J.L., Johnson, N.A., Watters, G.T., 2017. A revised list of the freshwater mussels (Mollusca: Bivalvia: Unionida) of the United States and Canada. *Freshw. Mollusk Biol. Conserv.* 20, 33–58.
- Woodruff, C.M., 1977. Stream piracy near the Balcones Fault Zone, central Texas. *J. Geol.* 85, 483–490.
- Woodruff, C.M., Abbott, P.L., 1979. Drainage-basin evolution and aquifer development in a karstic limestone terrain south-central Texas, U.S.A. *Earth Surf. Proc.* 4, 319–334.
- Zanatta, D.T., Murphy, R.W., 2006. Evolution of active host-attraction strategies in the freshwater mussel tribe Lampsilini (Bivalvia: Unionidae). *Mol. Phylogenet. Evol.* 41, 195–208.
- Zelditch, M.L., Swiderski, D.L., Sheets, H.D., Fink, W.L., 2004. Geometric Morphometrics for Biologists: A Primer. Elsevier Academic Press, San Diego, CA.

Supporting Information

Additional supporting information may be found online in the Supporting Information section at the end of the article.

Fig. S1. Phylogenetic tree reconstructed by Bayesian inference analysis for concatenated mitochondrial DNA and nuclear DNA (*cox1*, *nad1*, *ITS1* and *ANT*) sequence dataset.

Table S1. List of specimen information (species; source; DNA code; collected waterbody; state; GenBank accession numbers for cytochrome *c* oxidase I (*cox1*), NADH dehydrogenase I (*nad1*), internal transcribed spacer 1 (*ITS1*) and adenine nucleotide translocase (*ANT*); and morphometrics) used in the study.

Table S2. List of outgroup sequences used in the study.

Table S3. Substitution models for each gene partition used in the study.